ARL TECHNICAL REPORT 60-279



# ANALYTICAL STUDIES ON ION PROPULSION



R. H. Boden, et al



AUGUST 1960

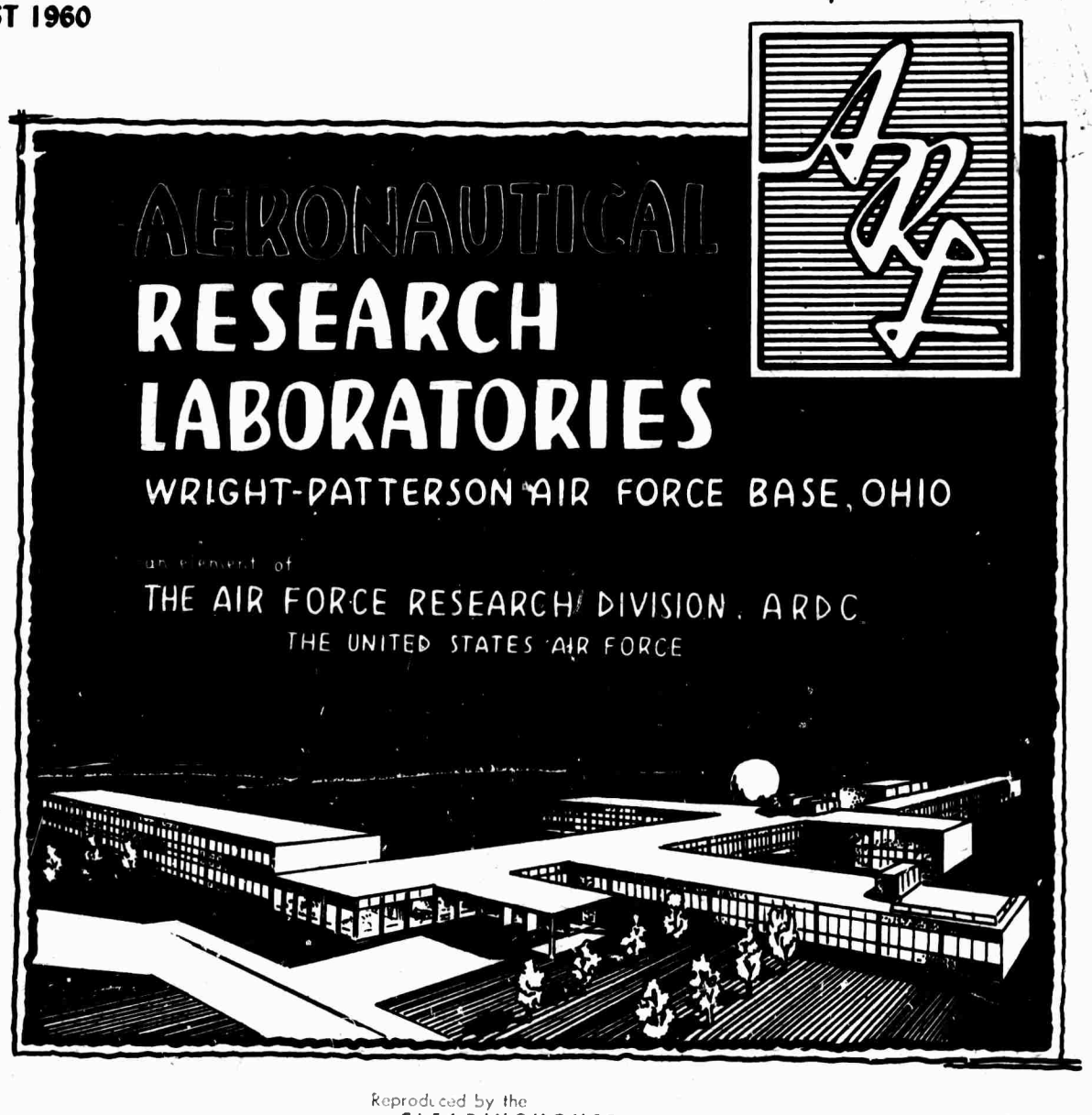

## NOTICES

When Government drawings, specifications, or other data are used for any purpose other than in connection with a definitely related Government procurement operation, the United States Government thereby incurs no responsibility nor any obligation whatsoever; and the fact that the Government may have formulated, furnished, or in any way supplied the said drawings, specifications, or other data, is not to be regarded by implication or otherwise as in any manner licensing the holder or any other person or corporation, or conveying any rights or permission to manufacture, use, or sell any patented invention that may in any way be related thereto.

---

Qualified requesters may obtain copies of this report from the Armed Services Technical Information Agency, (ASTIA), Arlington Hall Station, Arlington 12, Virginia.

---

Copies of ARL Technical Reports and Technical Notes should not be returned to Aeronautical Research Laboratories unless return is required by security considerations, contractual obligations, or notices on a specific document.

BLANK PAGE

ARL TECHNICAL REPORT 60-279

# ANALYTICAL STUDIES ON ION PROPULSION

*R. H. Boden*
*et al*

*Rocketdyne*
*A Division of North American Aviation, Inc.*

*AUGUST 1960*

Contract AF 49(638)-649
ARPA Order No. 6-58
Task No. 11

AERONAUTICAL RESEARCH LABORATORIES
AIR FORCE RESEARCH DIVISION
AIR RESEARCH AND DEVELOPMENT COMMAND
UNITED STATES AIR FORCE
WRIGHT-PATTERSON AIR FORCE BASE, OHIO

200 – November 1960 – 9-422

## FOREWORD

The studies described in this semi-annual report were made from July 1959 through December 1959, as part of the research on ion rocket engine systems supported by the United States Air Force through the Air Force Office of Scientific Research; Air Research and Development Command, under Contract No. AF49(638)-649. ARPA Order No. 6-58, Task No. 11.

Principal contributors to this report were: R. H. Boden, J. T. Congelliere, A. L. Cox, J. B. Denniston, S. L. Eilenberg, G. T. Harness, A. L. Huebner, T. W. Karras, B. T. Kimura, M. F. Kirby, V. R. Larson, T. M. Littman, E. Mayer, C. J. McDole, J. H. Molitor, D. D. Monaco, W. A. Moser, and G. W. O'Shaughnessy.

## ABSTRACT

Analyses of major problems associated with components of the ion rocket engine system have been made. Component studies include electrical power generation systems, thermal power conversion, and accelerating electrode configurations. Analyses of ion beam dynamics, propellant materials, radiation damage to working fluid for a nuclear power plant, and missions using low-thrust vehicles are presented. Interpretation of these analyses is made in terms of engine design parameters.

TABLE OF CONTENTS

## LIST OF ILLUSTRATIONS

LIST OF TABLES

# INTRODUCTION

Rocketdyne initiated its formal study program on ion rocket engines during the period from February 1957 to January 1958 under Contract AF49(638)-16.

Upon completion of the analytical study, a final technical report was issued (Ref. 1). The scope of the report included the complete engine system and its components from the heat source to the exhaust jet, as well as the determination of engine thrust level requirements for interplanetary missions.

Based upon the analyses carried out during the first year of study, it was possible to formulate a program for continued analytical studies, as well as to define an approach toward an experimental ion thrust chamber program. Consequently, analytical studies of the ion rocket engine were continued under Contract AF49(638)-344 and subsequently under Contract AF49(638)-649. A final technical report was issued covering the period from March 1958 through February 1959 which summarized the analyses of missions using low-thrust vehicles, and of ion rocket components (such as reactors) as power sources, mechanical power conversion, direct power conversion, electrical power generation systems, and accelerating electrode configurations (Ref. 2). It is the purpose of this technical report to summarize the research studies performed under Contract AF49(638)-649 from 1 July through 31 December 1959.

## THE ION THRUST DEVICE

### ACCELERATOR GEOMETRY STUDY

The shaping of electrodes to produce a well-collimated ion beam is the initial problem in developing an ion thrust device. Once an electrode shape has been established, it must then be evaluated for propellant ionization efficiency, ion emission uniformity, power efficiency, thrust efficiency, electrode erosion rate, neutralization electron flowback, and factors affecting a stable thrust level.

Because the proper choice of electrodeconfigurations for the ion accelerating system is critical if high efficiency and long operation lifetime are to be accomplished, a precise knowledge is required of the electric field distribution in the region of the ion beam. The descriptions of the field distribution, obtainable from analytical solutions of Poisson's equation ($\nabla^2 V = -\rho/\epsilon$) are well known for only a few special diode geometries, such as parallel planes, concentric spheres, concentric cylinders, and Pierce geometries. Although it is possible to solve Poisson's equation mathematically using these particular shapes (Ref. 3, 4, and 5), for complex geometries, theoretical analyses become so complex that it is necessary to resort either to approximation methods or to simulation techniques.

To study the influence of electrode geometry on such factor as the space charge current limitation, beam focusing and beam spreading, an ion thrust chamber simulator, as shown in Fig. 1, was designed (Ref. 2) during 1958, and constructed under the current contract.

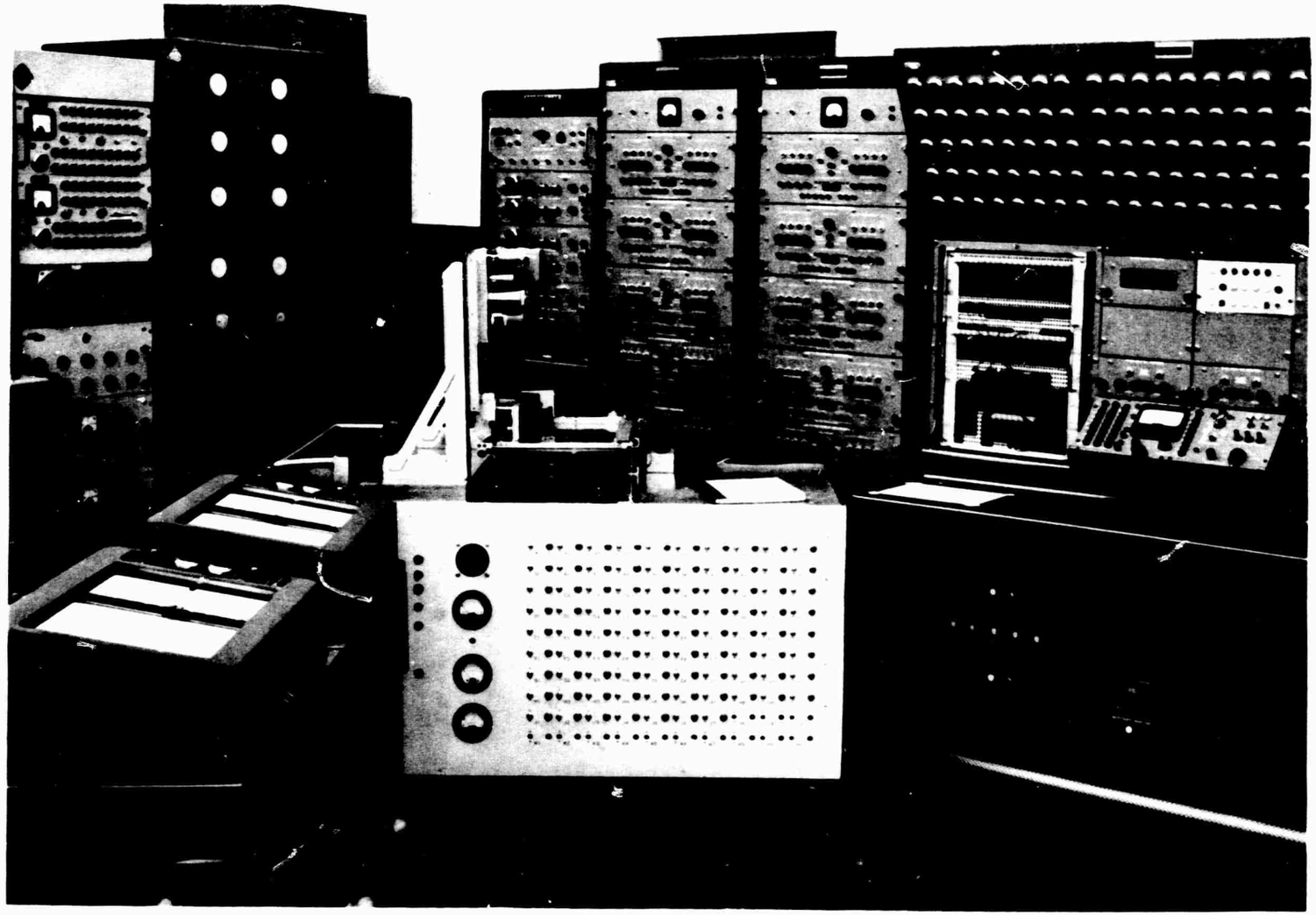

Figure 1. Ion Thrust Chamber Simulator

Test runs were made in the electrolytic tank using a simple diode geometry. The results obtained from these tests clearly showed that the tank components had to be improved before this technique could be extended to produce accurate designs for complex electrode systems. An improved sensing head was designed and built, and changes were incorporated in electrical circuits to increase the signal-to-noise ratio. Subsequent tests showed that the difficulties had been cleared up and trajectories were successfully plotted.

Resistance-paper techniques have been used to study field distributions in the interelectrode space and in the neutralization region. The results of this work are described in the section on beam neutralization study (page 9). These techniques do not permit the inclusion of space charge effects, but constitute a reasonably rapid method of estimating the focusing properties of electrode geometries. These techniques are particularly useful in the period before the electrolytic tank can be effectively utilized for this work.

The remainder of the current contract period will be utilized to investigate the effect on ion optics of electrodes having complex geometrical shapes.

Two basic accelerator geometries are being considered; namely, the accel-decel geometry (Ref. 6), and the modified Pierce geometry (Ref. 7). The accel-decel geometry is of interest because it offers a way of eliminating electron flowback, and might be capable of exhibiting a higher perveance than Pierce accelerators.

The Pierce geometry, on the other hand, is a simpler system than the accel-decel, and it has been shown, theoretically, that electron flowback can be prevented in this system by proper ion beam collimation and electron emitter positioning. Furthermore, there is reason for doubt that the accel-decel system can appreciably increase perveance over that of the Pierce; and even if it did, this may be offset by power losses resulting from excess ion beam compression.

Thus, the problem of determining the nature of practical electrode geometries reduces to a search for and evaluation of all significant factors which accompany the operation of an ion thrust device in free space.

The study program has been divided into two efforts: (1) study of the phenomena occuring within the accelerator region, such as power loss through beam compression, power loss by thermal radiation, electrode erosion by sputtering processes, scattering of ions by neutrals, thermionic emission from electrodes, thermal beam spreading, and photoelectric emission and (2) study of the beam dynamics in the external electrode region including beam neutralization and beam stability.

## BEAM COMPRESSION POWER LOSS

As the positive charged ion beam is ejected from the acceleration region, it carries with it electrical energy arising from the interaction of the individual ions. The energy content of the beam increases as it is compressed. This energy is unavailable for the production of thrust so that this must be taken into consideration in the determination of power efficiency.

The power carried away by the ion beam is calculated by integrating the energy contained throughout an element of the beam, and then multiplying this energy by the rate at which the elements are expelled. The energy per element was integrated by an approximation method, and the power loss was determined. The details of this calculation will be published in a technical note.

It was found that the percent of power loss resulting from this mechanism increases rapidly with the perveance of a Pierce geometry rising to 10 percent or more. From this analysis there arises the question of whether the

theoretical advantage in the increase of perveance produced by accel-decel system might be offset by beam compression losses. This problem will be explored by (1) determing through resistance-paper analog studies, whether the increased perveance can be obtained, and (2) calculating beam compression losses at the higher perveances.

## THERMAL RADIATION LOSSES

A major source of power loss in the accelerator region is a result of thermal radiation from high-temperature surfaces. The ionizer surface is the hottest portion of the accelerator system. However, a poor structural design may produce large radiation losses from the larger surface areas presented by the accelerating electrodes, focusing electrodes, or heat shields, even though they may be at lower temperatures.

This study considers the losses from the ionizing surface only. The best available data on surface emissivity of porous tungsten, ionizer temperatures, and Langmuir's cylindrical diode equations were combined to form an expression for the ratio of thermal loss to the beam power.

It was determined that the proportion of power loss is inversely proportional to the fifth power of specific impulse. Hence low specific impulses can be accompanied by lowered efficiency. For example, a typical geometry designed for a specific impulse of 10,000 sec with an ionizer surface temperature of 1500 K has an efficiency of 83 percent. The radiation loss ratio is also reduced by increasing perveance as is suggested by proponents of the accel-decel system, but this advantage may be nullified by beam compression losses.

This study is nearly completed.

## SPUTTERING

The erosion of the accelerating electrodes by sputtering processes can degrade the performance of the ion engine and can ultimately destroy it. Since the ion engine must operate for an extended length of time, the rate of electrode erosion is a very important factor in determining the length of time the engine can efficiently operate.

It is necessary to find data on the number of electrode atoms which will be sputtered away by a single impinging ion. Unfortunately, data obtained by experiment have been, until recently, obtained for ion energies considerably less than the energies of interest (less than 500 ev), and for ions other than those generally applicable as an ion propulsion propellant. The recent data have been taken at energies up to about 40 kev. This information is discussed in detail in a forthcoming technical note. The low-energy sputtering data accumulated before 1955 have furnished information on the sputtering ratio (atoms per ion) as a function of various parameters. In summary, the sputtering yield increases with ambient gas pressure, angle of incidence, ion energy, target temperature, and ion mass; it varies with electrode surface condition, and weight of sputtered atoms; and it is independent of the ion density.

Recent work (Ref. 8) has shown, theoretically, that at high energies the sputtering yield increases with ion mass and decreases inversely with the sputtered atom mass and ion energy. This decrease with energy occurs because the incident ion penetrates deeply into the electrode material, so that little energy is lost in the surface where atoms are normally sputtered. This conclusion was partially born out by experimental work performed by D. E. Harrison of the University of Toledo. He used copper as a target, and beamed ions such as hydrogen, argon, krypton, and uranium which produced sputtering ratios of 0.01, 9.02, and 20.9 at 30 kev, respectively.

The impingement of ions upon the accelerator electrode, therefore, must be kept to a very low rate. Experimental data obtained at Rocketdyne have indicated that sputtering ratios of 10 atoms per ion may be encountered. Thus, a very small fraction of one percent of the beam can be allowed to impinge upon the accelerator electrode. It is theoretically possible to design an electrode geometry so that no ions will impinge upon the accelerator. If this is done, there still will be a source of impinging ions. This is the subject of the following two sections.

## THERMAL ION MOTION

This study is still in process, but preliminary results show that a highly compressed ion beam can produce thermal velocities equal to nearly 10 percent of the velocity imparted by the accelerator. To avoid ion impingement resulting from thermal ion beam spreading, analytical designs must include extra clearance for the ion beam when it is highly compressed. This study is continuing.

## ION-NEUTRAL COLLISIONS

Because a fraction of the propellant is not ionized, there will be an accumulation of neutral atoms in the accelerator region. Some of the accelerated ions will collide with these neutrals and be scattered. The differential scattering cross section for ions on atoms (Ref. 9) shows that the elastically scattered particle is most likely to move in the direction of the ion beam. Thus, for this scattering involving equal masses, the ion will come to a rest, and then most likely will be accelerated into an electrode with an energy, on the average, below the total accelerator potential. The scattered neutrals will be scattered through a cone defined by the edges

of the ion beam at the ion emitter; again, their average energies will be below the total accelerator potential. These scatterings will increase in number as the ion beam density increases. This study is continuing.

## BEAM NEUTRALIZATION STUDY

The beam neutralization study has been a major theoretical effort under the present contract. The problem is to obtain charge neutrality of the vehicle and of the exhaust. Without neutrality, there would very quickly be no thrust because of the strong attractive force which would build up between the ions in the beam and the negatively charged vehicle.

Studies to date strongly indicate that this neutralization can best be accomplished by injection of electrons into the positively charged propellant beam, just downstream of the accelerating electrode. In this region and beyond, the ion-electron beam will then form a complex dynamical system of interacting charged particles.

A thermionic emitter, properly heated, can easily supply the electron currents needed, and calculations performed under the current contract indicate that the net positive charge of the beam will draw the electrons into the ion region. The details of this analysis are to be published in a technical note. An exact mathematical solution of ion and electron motion requires the simultaneous solution of the following three equations:

$$\nabla^2 V = \frac{\rho_T}{\epsilon_0} \tag{1}$$

$$\left(\frac{d}{dt}\right) \vec{V} = \left(\frac{q}{m}\right) \overrightarrow{\nabla V} \tag{2}$$

$$\vec{i} = \rho_e \vec{V} \tag{3}$$

where V is the potential field, $\rho_T$ is the total charge density (ion and electron), $(\frac{q}{m})$ is the charge-to-mass ratio of the charged particle, $\overline{V}$ is its velocity vector, $\overline{i}$ is the electron current, and $\rho_e$ is the electron charge density. The required solution must satisfy not only the required condition of total charge neutrality, but also the boundary conditions imposed by the accelerating system (ion emitter, focusing electrode, and accelerating electrode).

An ideal solution of the neutralization problem has been obtained by considering an ideal electron injection geometry consisting of two flat infinite emitter surfaces located on both sides of an infinite slab of positive ions with uniform density. The electrons are injected into the positive ion slab and proceed to oscillate back and forth across the slab. The number of electrons injected is controlled so that the total electron space charge is equal to the total ion space charge. This is the condition required for neutralization.

Using this ideal setup, Poisson's equation was solved. The results of this calculation are shown in the following curves:

Figure 2 shows the ratio of the electron charge density $(\rho_e)$ to the electron charge density at the center of the beam $(\rho_d)$ as a function of distance $(x)$ for a given slab width (d-s) and electron emitter-to-slab-edge distance (s).

Figure 3 shows the ratio of the electric field potential (V) to the electric field potential at the center of the beam $(V_m)$ as a function of distance (x) for a given slab width (d-s) and electron emitter-to-slab-edge distance (s).

Figure 4 shows the ratio of the ion beam charge density $(\rho)$ to the electron-charge density at the center of the beam $(\rho_d)$ as a function of slab width and electron emitter-to-slab-edge distance.

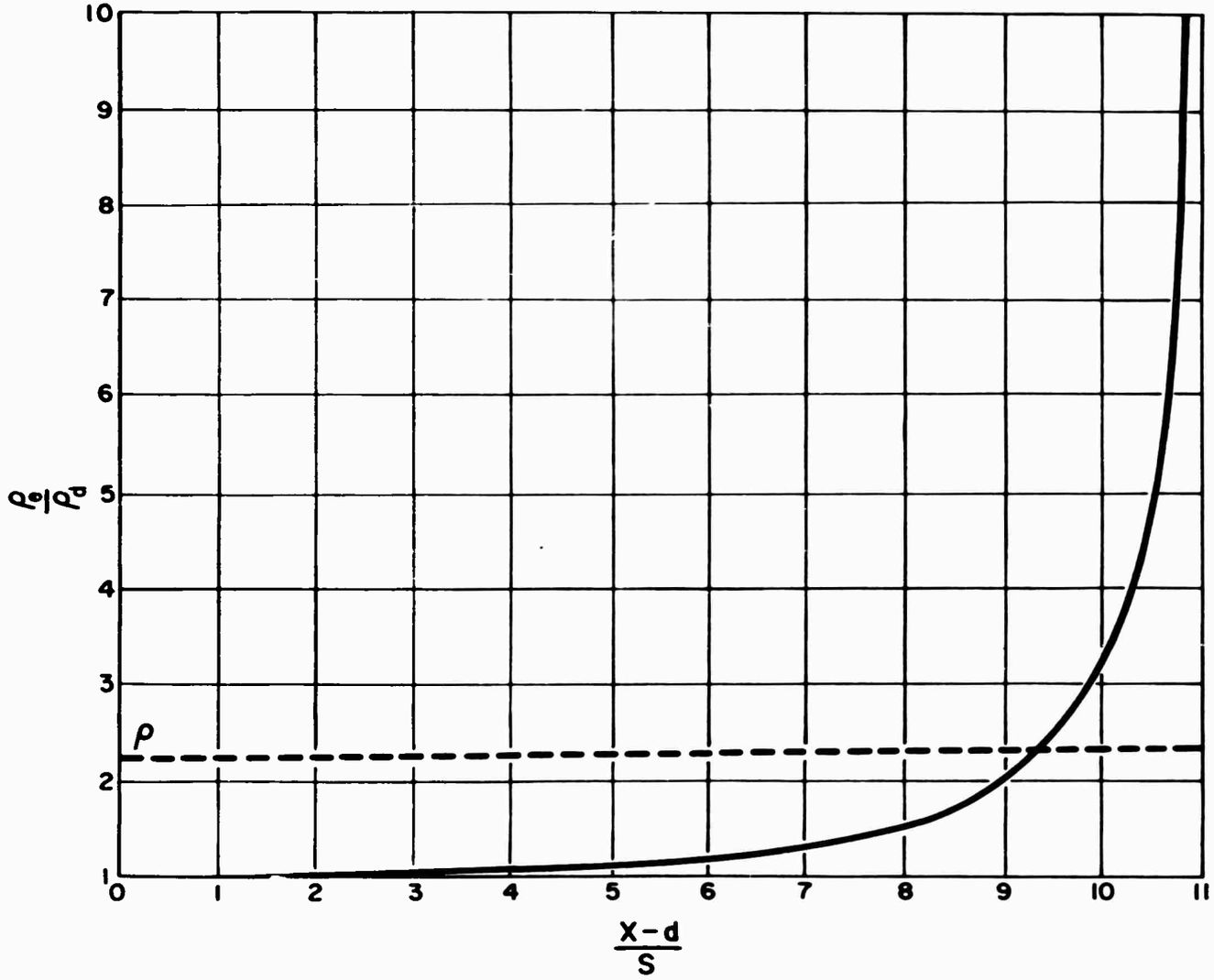


Figure 2. Electron Charge Distribution

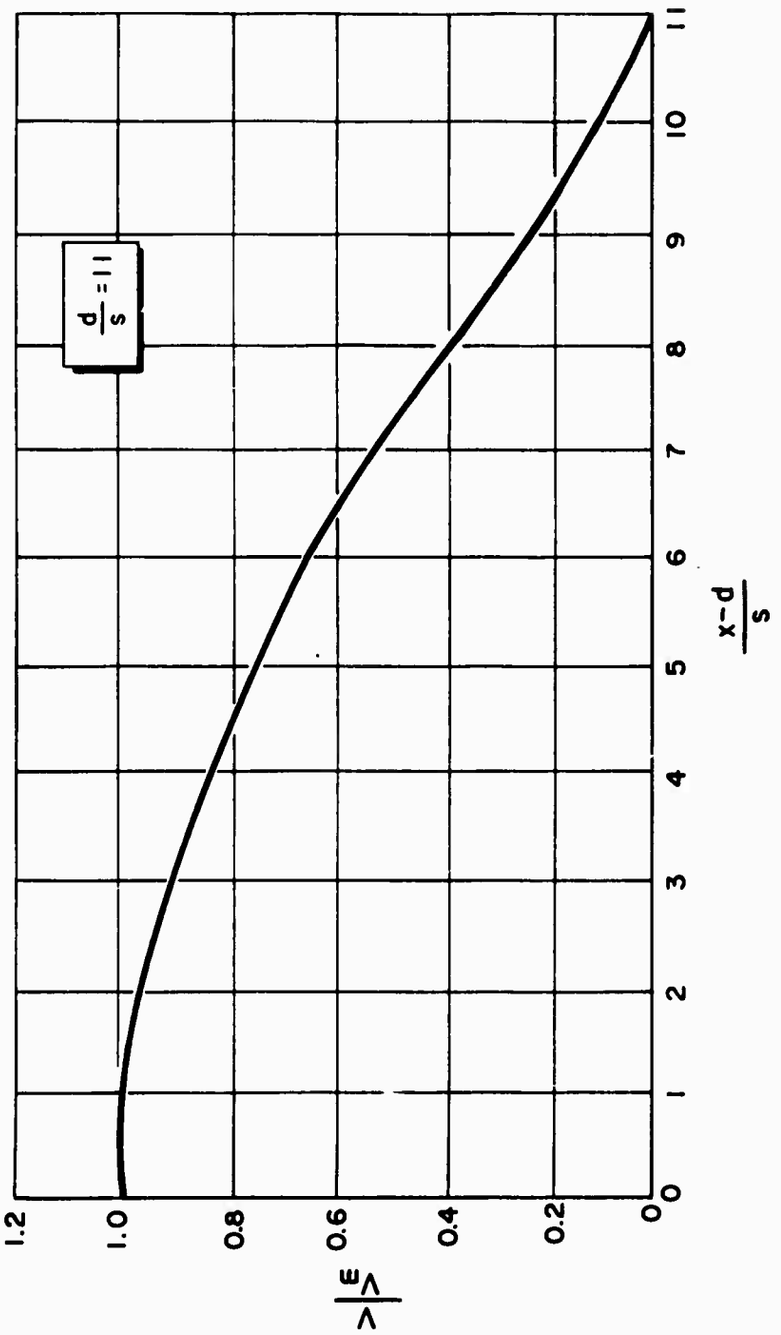


Figure 3. Potential Distribution

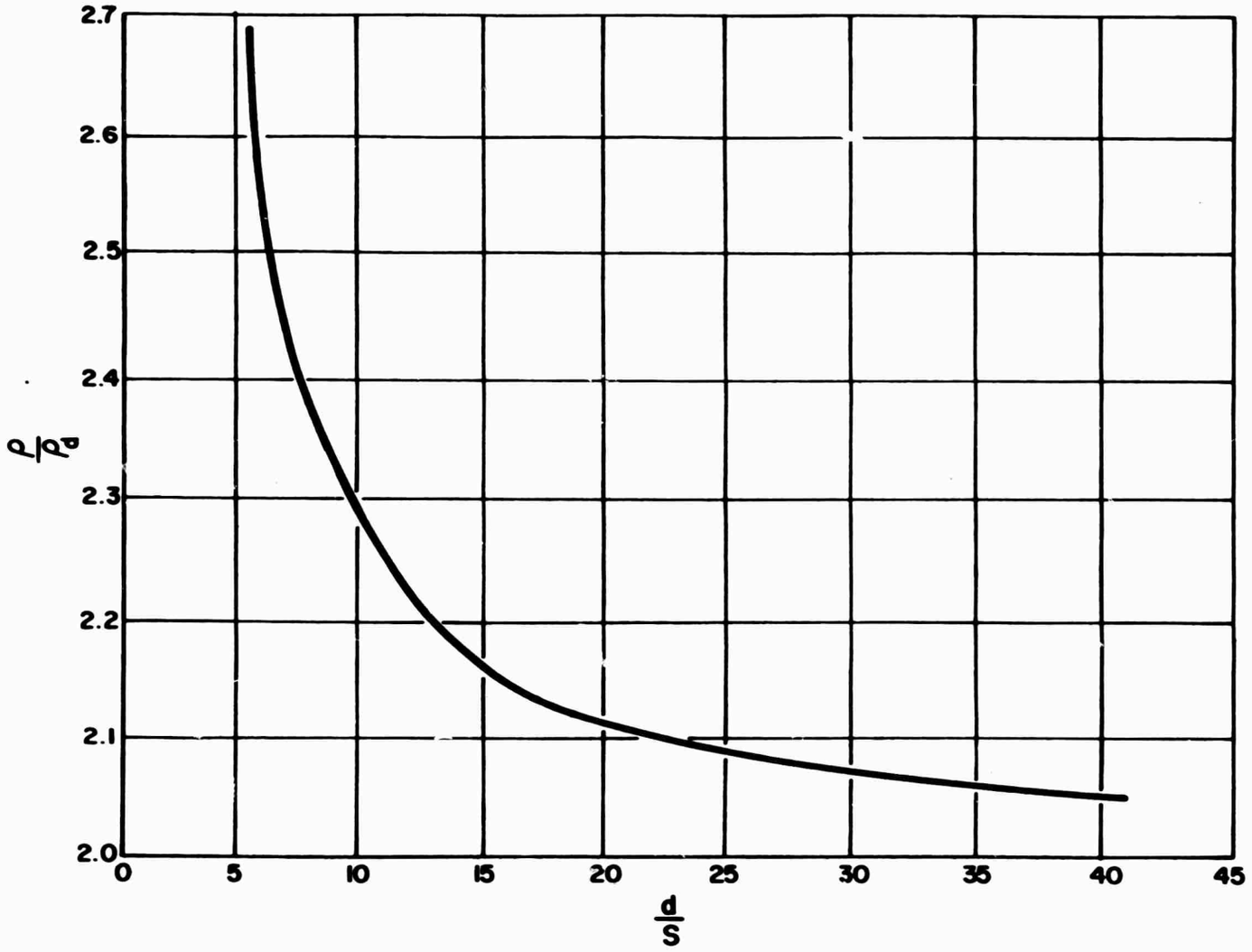


Figure 4. Electron Charge Density Variation (Center of Beam)

Figure 5 shows the electric field potential at the beam center ($V_m$) as a function of slab width (d-s).

The electric field of the positive ions is not the only force acting on the neutralizing electrons. The field produced by the accelerating electrodes extends beyond the thrust chamber, and can also affect the electron trajectories.

A preliminary study of these electrode fields was made using resistance-paper techniques. The field of a Pierce-type geometry was used as a representative electrode system.

The field patterns obtained are shown in Figures 6 and 7 for an enclosed accelerator (a vehicle of the smallest size possible) and in Figure 8 for an accelerator behind an infinite plane (a ship of the largest size possible). Figure 9 shows how the fields fall off with distance from the vehicle.

One particularly crucial problem associated with neutralization is the determination of whether some, or all, of the injected electrons will be directed upstream to the ion emitter by the electric fields. This effect is undesirable because it results in excessive and probably non-uniform heating of the ionizer, and excessive current drainage through the generator. It conceivably could prevent complete neutralization of the ion beam.

The electrons will be prevented from travelling upstream if the electric field near the exit aperture presents an electric potential barrier to this motion. The accelerator-decelerator technique has been proposed as a method for producing a barrier by introducing another electrode at a negative potential upstream from the final or decel electrode. This results in a reverse field which repels the electrons so that they will travel only downstream.

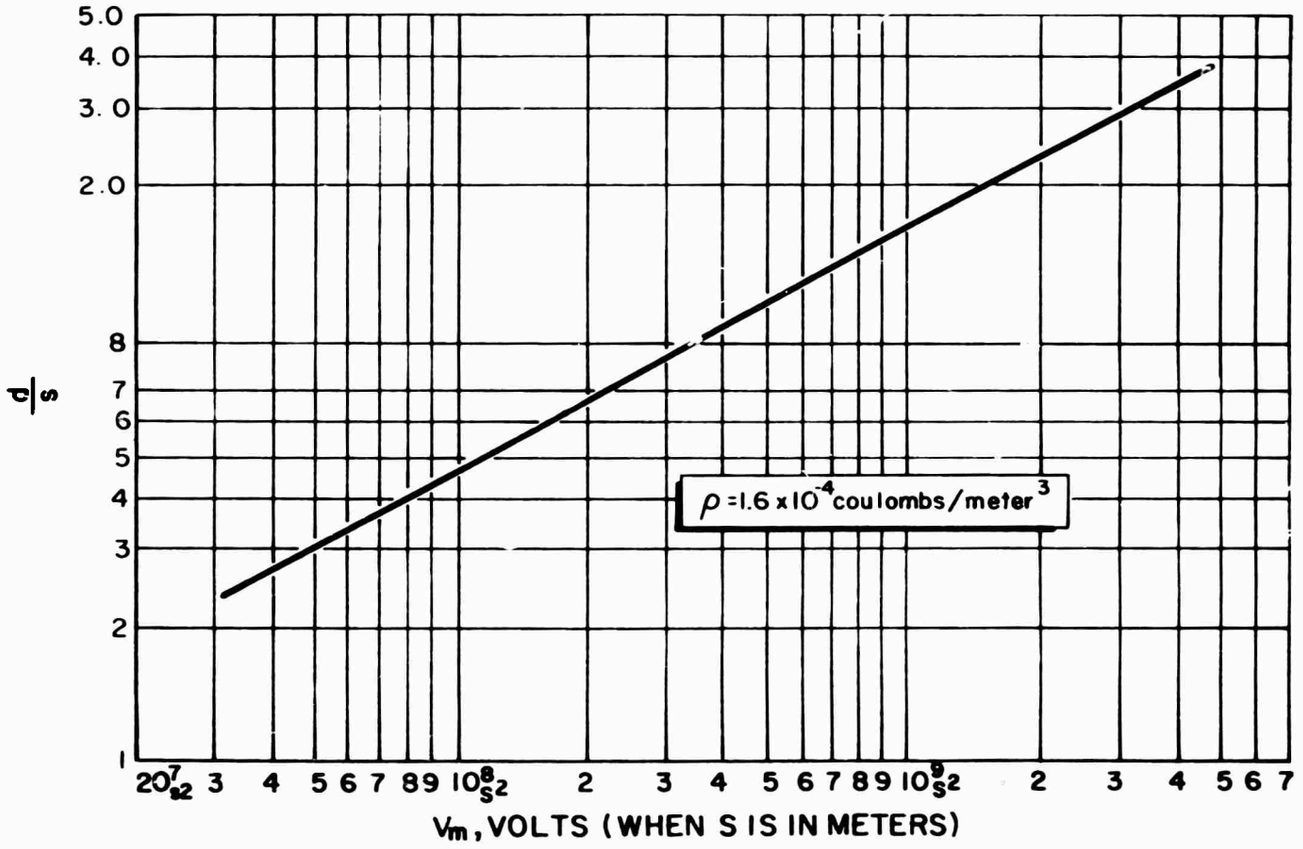


**Figure 5. Potential Variation (Center of Beam)**

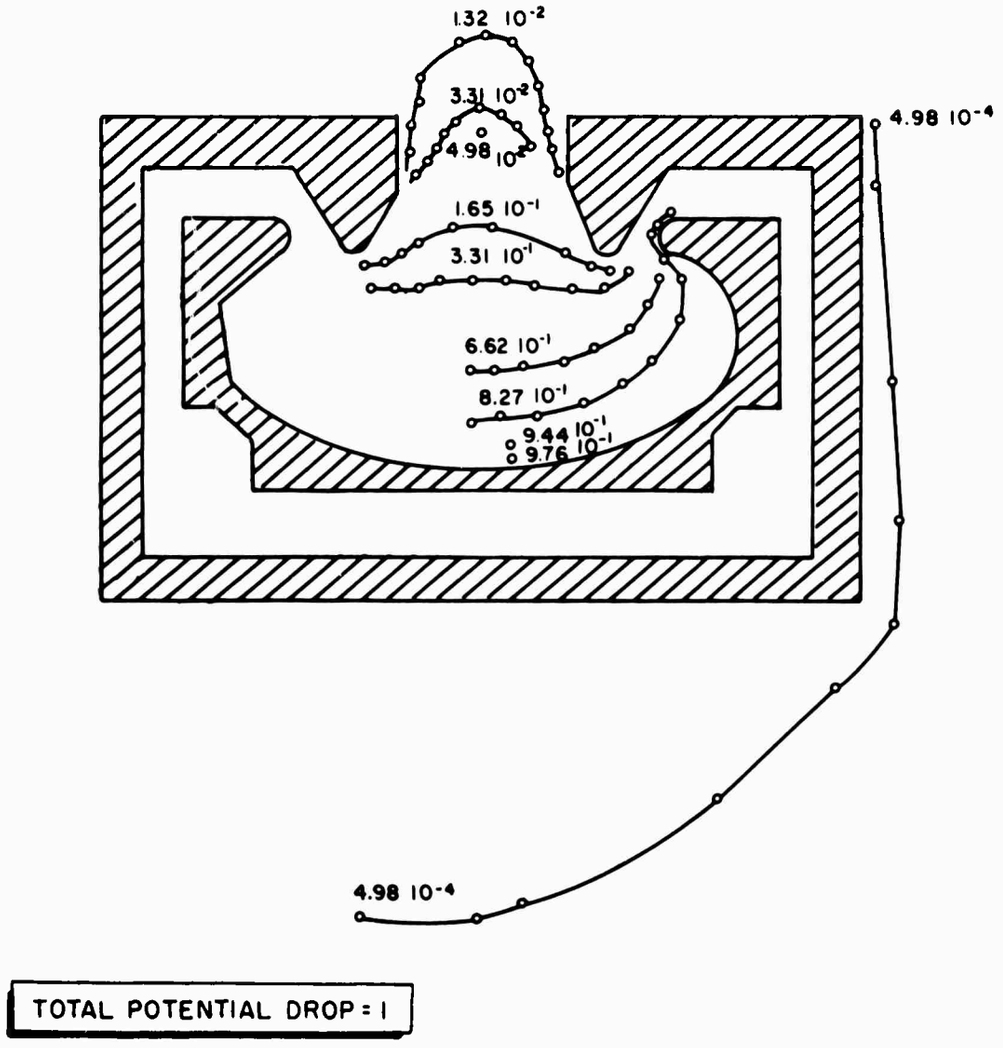


Figure 6. Potential Distribution for Pierce-Brewer Geometry

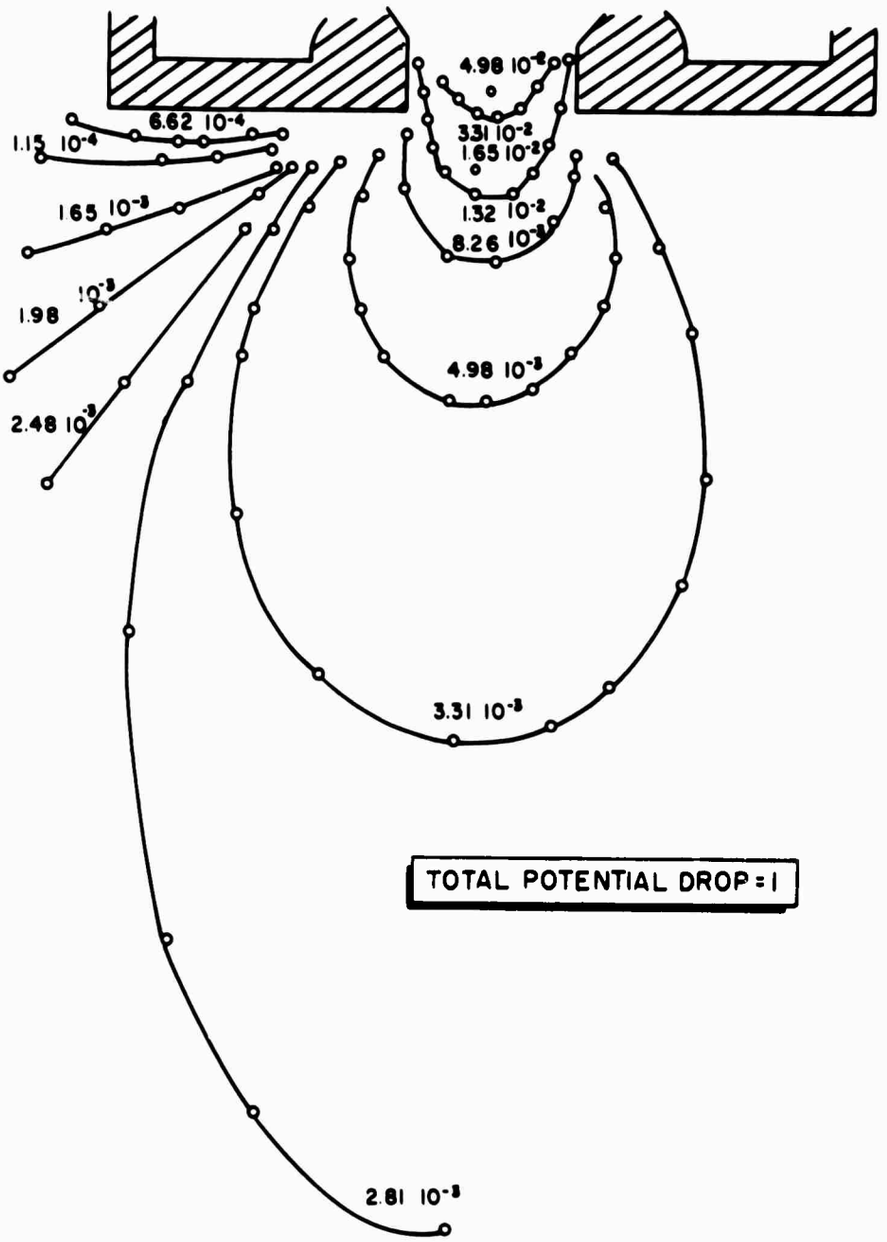


Figure 7. Potential Distribution for Pierce - Brewer Geometry

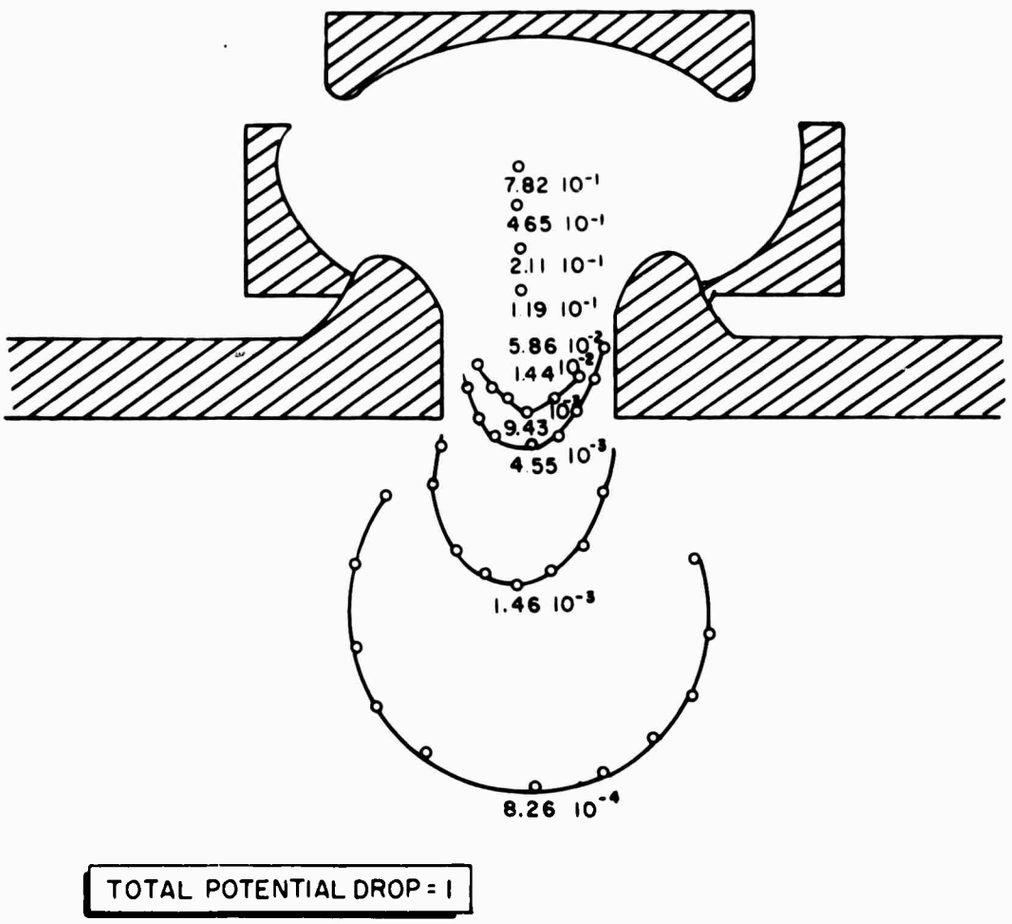


Figure 8. Potential Distribution for Pierce - Brewer Geometry with Infinite Accelerating Electrodes

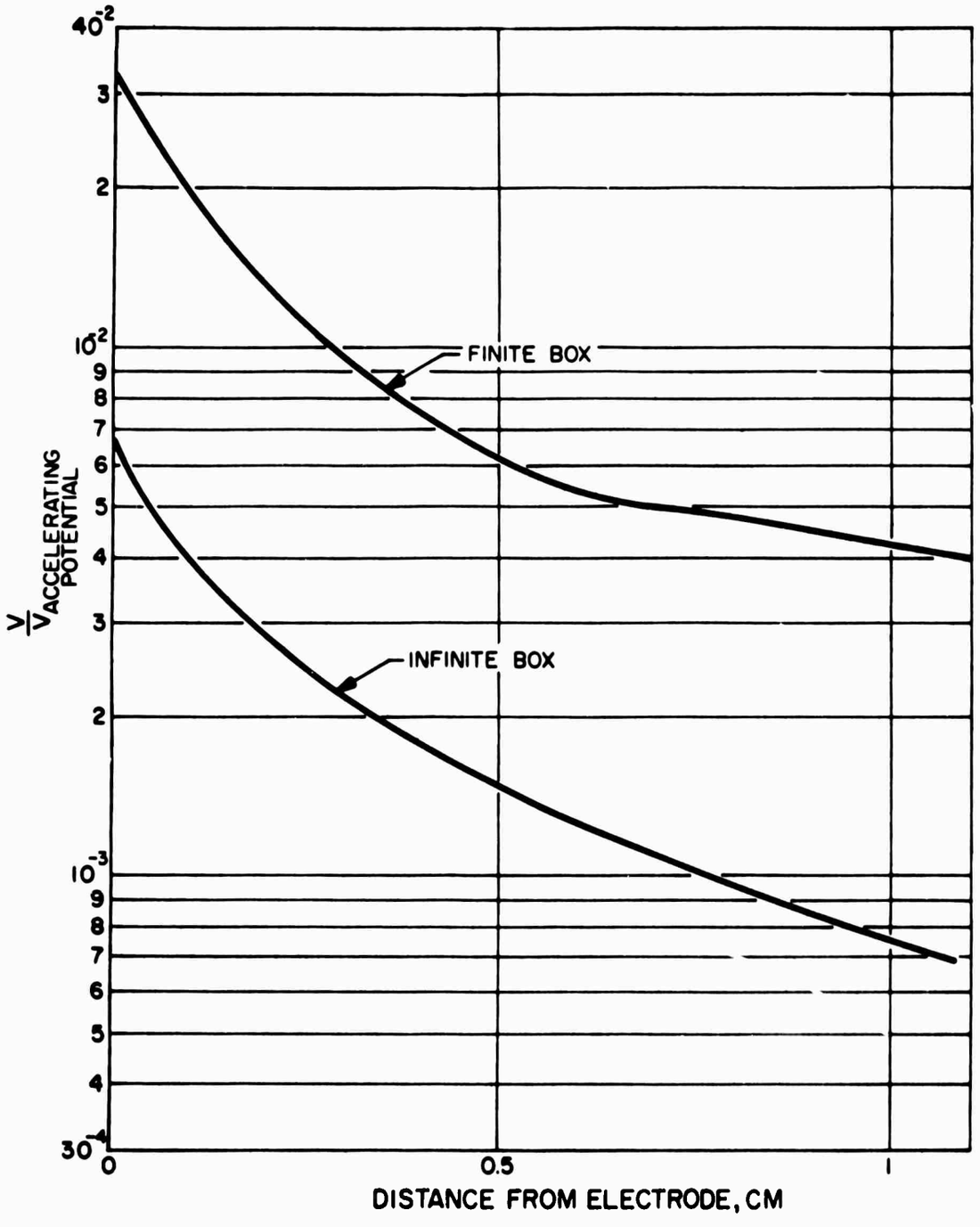


**Figure 9. Potential vs Distance from Accelerator**

It would be desirable, though, to be able to produce a barrier without the use of an extra electrode. The addition of another electrode complicates the present problem of finding the shape and spacing of the electrodes which produce the required degree of focusing and uniformity of emission from the ion source. The additional power supplies required for the additional electrodes will add mass and complexity to the final system.

A study has been conducted to determine the possibility of forming a barrier with only two electrodes (ion emitter and accelerator) being present.

It is characteristic of a diverging beam of charged ions that an axial gradient is produced which will accelerate injected electrons back to the ion source. As a corollary to this, a converging beam produces an axial field which will accelerate the electrons downstream along with the ejected ions. Thus, a barrier may be produced by simply converging the ion beam.

To substantiate this conclusion, calculations were made of the rate of spread of an ion beam, and Poisson's equation was solved inside a beam that first converges, then diverges. The results show that convergence of less than 1 deg will provide fields sufficient to direct the electrons away from the thrust device.

Figure 10 shows the variation of both the electrode potential (see Fig. 9) and the potential due to beam convergence. From the slopes of these curves, the field strength due to each source was calculated, and the optimum injection distance determined. In this case, it was seen that for an injection distance of 5 to 7 mm the electrons would be forced downstream with a minimum of additional velocity.

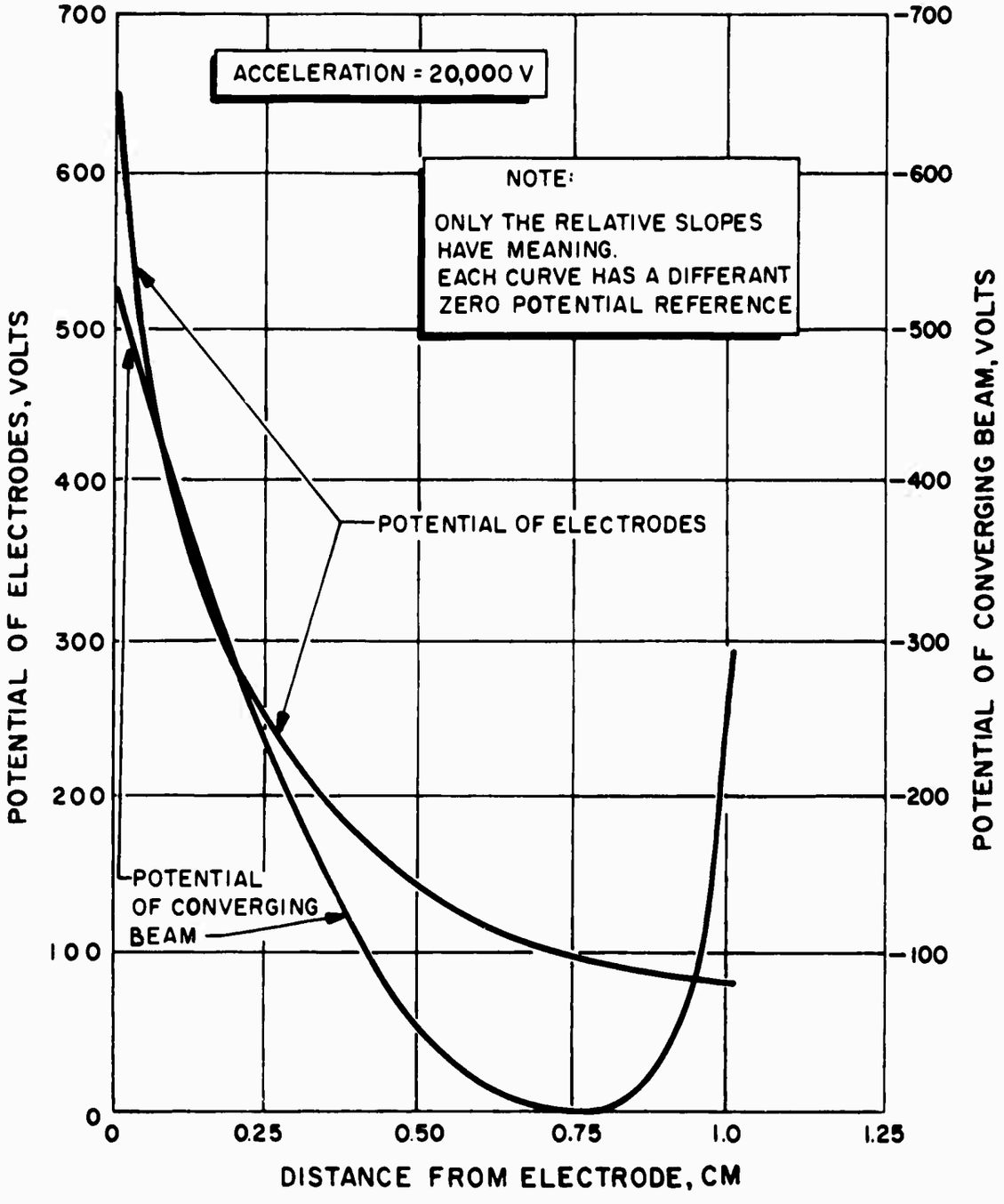


Figure 10. Potential vs Distance from Accelerator

## BEAM STABILITY

Along with the neutralization studies, the dynamics of the beam after the neutralization are being analyzed. Beam instabilities, such as oscillations or transients, can give rise to field variations near the critical electron injection region. If the field variations are severe, the field barrier may periodically or permanently be reduced or eliminated. Thus, the electrons will be free to flow back to the ionizer, resulting in damage and uncontrolled thrust variations.

To determine whether such instabilities exist, it is necessary to analyze the dynamics of the beam. Unless microscopic neutrality exists, the beam itself will oscillate. Calculations of beam neutrality have shown that the charge distribution is initially nonuniform across the beam. As the charge distribution tends toward thermal equilibrium, this inhomogeneity will disappear. The time required to reach an equilibrium state has been calculated. These preliminary calculations show that radiation losses (Bremsstrahlung) and electron-ion collisions require long times to bring about equilibrium, and that even electron-electron collisions require many milliseconds to produce microscopic neutrality. Consequently, the ion beam, though grossly neutralized, will travel a considerable distance, during which time the beam oscillations will occur.

Calculations have shown that unstable longitudinal oscillation of the gross beam will not take place in the interval between electron injection and equilibrium. A similar analysis will be performed during the current contract period to determine whether the transverse oscillations are also stable.

# SELECTION AND IONIZATION OF MOLECULES AND COLLOIDS FOR ELECTRICAL PROPULSION

## INTRODUCTION

The power for acceleration of ions decreases rapidly with ion weight (Ref. 10); therefore, the possibility of employing molecular or colloidal ions as the propellant in ion rockets has been examined to extend the possible ion weights above the maximum atomic weight.

The heavy-ion engine is applicable to the specific impulse range and shorter flight time characteristic of the plasma engine and the lower values achievable by the atomic ion engine (Fig. 11) (Ref. 11). The heavy-ion engine, like the cesium engine, is power limited and will probably operate at the space charge limit; however, the optimum perveance for these heavy ions varies from that of the cesium ion beam to several orders of magnitude lower. Therefore, the design parameters, slit length and interelectrode spacing, assume more practical values for low specific impulse missions operating with heavy ions. As an example of an ion rocket flight, a round-trip lunar mission is considered at two different values of G, and the possible operating parameters are presented in Table 1. The performance of propellants with different charge-to-mass ratios in a 10-ton vehicle with a 200-kw powerplant operating at 70-percent power efficiency and weighing 20 lb/kw is shown. An approximate $\Delta$ v value of 32,000 ft/sec was employed.

Molecules can undergo bond rupture; therefore, the study of molecular ions introduces a new problem not encountered in the production of atomic ions. The selection of materials for preparation of stable positive and negative molecular ions, methods of ionization which ensure their formation without

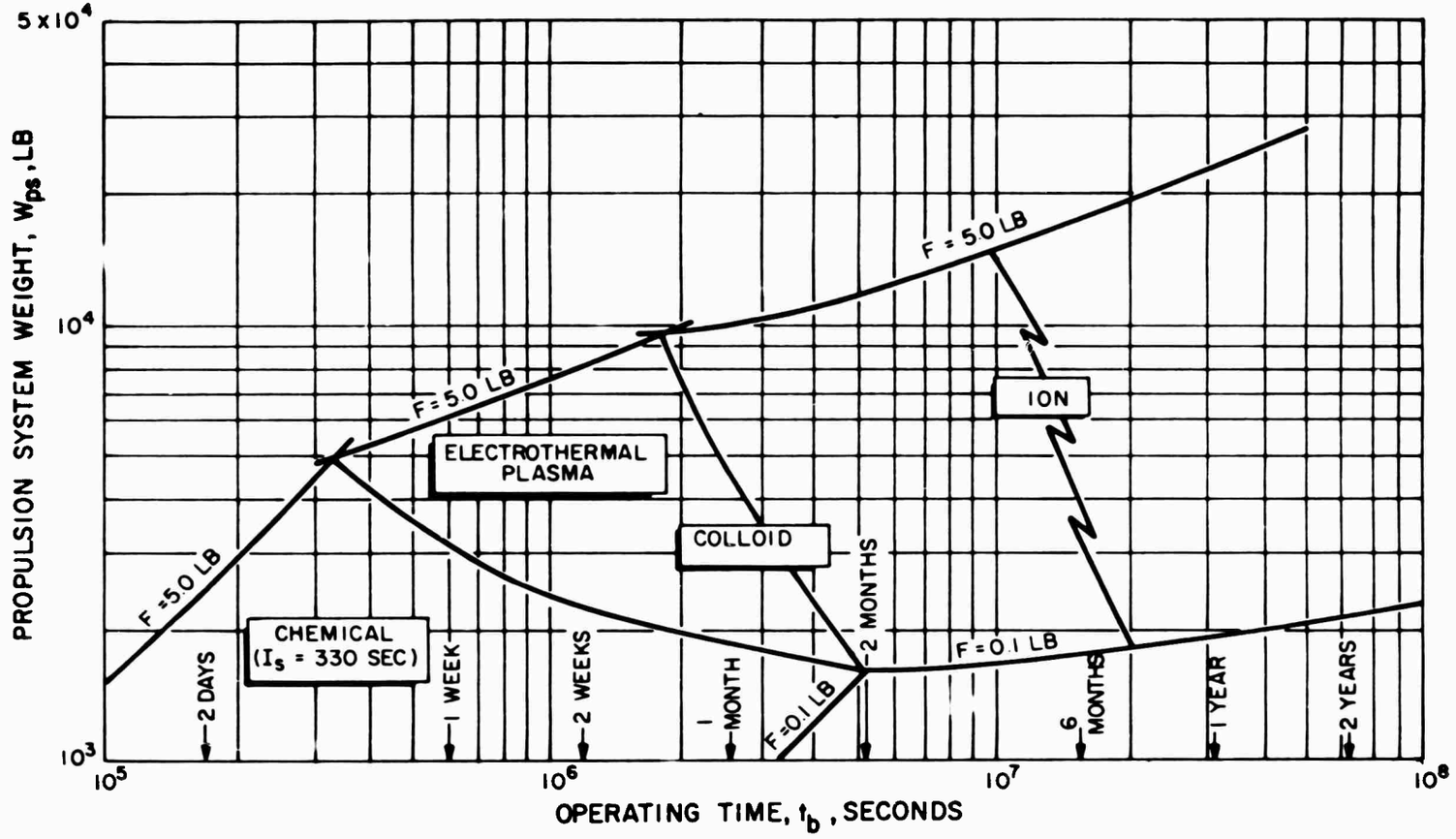


Figure 11. Competitive Operating Regimes of Several Low-Thrust Space Rockets

TABLE 1

OPERATING PARAMETERS F

ROUND TRIP MOON MISS

| Thrust-to-Weight Ratio G | Specific Impulse $I_s$, sec | Thrust, F, lbs-f | Final Weight $W_f$ tons | Propellant Weight $W_p$ tons | Payload Weight W tons | Burning Time $t_b$ months | Char Mass Elec per |
|---|---|---|---|---|---|---|---|
| $10^{-4}$ | 3200 | 2 | 7.4 | 2.6 | 5.4 | 3.2 | 7.52 (C 1.67 (M.W (M.W |
| $2 \times 10^{-4}$ | 1610 | 4 | 4.8 | 5.2 | 2.8 | 1.6 | 7.52 (C 1.67 (M.W (M.W |

TABLE 1

OPERATING PARAMETERS FOR A ROUND TRIP MOON MISSION

| Payload Weight W tons | Burning Time $t_b$ months | Charge-to-Mass Ratio $\alpha$ Electronic Charges per Atomic Mass unit | Accelerating Voltage V kilovolts | Interelectrode Spacing d cm | Slit Length h cm |
|---|---|---|---|---|---|
| 5.4 | 3.2 | $7.52 \times 10^{-3}$ ($Cs^+$) | 0.63 | 0.064 | 1560 |
| | | $1.67 \times 10^{-3}$ (M.W. = 600) | 3.1 | .29 | 345 |
| | | $10^{-3}$ (M.W. = $10^{-3}$) | 5.2 | .48 | 210 |
| | | $10^{-4}$ | 52 | 4.8 | 21 |
| | | $10^{-5}$ | 520 | 48 | 2.1 |
| | | $10^{-6}$ | 5200 | 480 | 0.21 |
| 2.8 | 1.6 | $7.52 \times 10^{-3}$ ($Cs^+$) | 0.171 | 0.0112 | 8900 |
| | | $1.67 \times 10^{-3}$ (M.W. = 600) | 0.77 | 0.051 | 1960 |
| | | $10^{-3}$ (M.W. = $10^{-3}$) | 1.29 | 0.084 | 1190 |
| | | $10^{-4}$ | 12.9 | 0.84 | 119 |
| | | $10^{-5}$ | 129 | 8.4 | 11.9 |
| | | $10^{-6}$ | 1290 | 84 | 1.19 |

BLANK PAGE

fragmentation, and methods for producing colloidal ions have been investigated. A more detailed discussion of these topics is being prepared as a technical note.

## SELECTION OF MATERIALS FOR PRODUCTION OF MOLECULAR IONS

Because any ion propellant that is a mixture of particles of different charge-to-mass ratios is inefficient in utilization of power and propellant material (Ref. 12), fragmentation of molecules must be avoided. Hence, the structural stability of molecules is a decisive factor in the selection of materials for molecular ion propellants. Structural stability has been evaluated in conjunction with consideration of the temperature at which the substance can produce a sufficient vapor pressure for operation of an ion engine.

Ease of ionization and avoidance of multiple ionization pose a second basis for the selection of materials for ion propellants. Investigation has revealed that organic compounds having a high degree of resonance stabilization fullfill the requirements of high structural stability. These include the condensed aromatic ring compounds, organometallic compounds of the ferrocene and metal phthalocyanine types, silanes, biphenyl, heterocyclic compounds, free radicals, aromatic phospinic nitrides, and dyes, particularly of the quinone type. Data on ionization potentials are not available for all of these types of compounds, but in all cases where data exist (Ref. 13 and 14), they exhibit lower ionization potentials than the 12 ev of the average c-c bond. Even less information on electron affinities is available, and of the selected classes of compounds, only values for the condensed aromatic ring compounds have been reported. In this type of compound the ionization potentials decrease and electron affinities increase with increasing molecular weight. Such a compound, $C_{34}H_{18}$, has an ionization potential of 6.04 ev and an electron affinity of 3.89 ev. Completely fluorinated

derivatives of the selected classes of compounds are expected to have high electron affinities, and the aromatic resonance stabilization and opportunities for energy redistribution should enable these molecules to resist fragmentation or electron detachment.

Individual members of the classes of compounds selected on the basis of structural stability and ease of ionization have been evaluated in regard to chemical inertness, molecular weight, density, toxicity, availability, and cost.

## METHODS OF PRODUCING IONS

Electron bombardment of molecules can produce negative or positive ions depending on the energies of the bombarding electrons, but the electron energies must be carefully controlled to avoid fragmentation. The efficiency of the ionization process is favored by the large cross sections of heavy molecules. For positive ion formation, the electron energy should be slightly greater than the ionization potential of the substance, but for negative ion production, the attachment cross section increases with decrease in energy of the electrons. Hence the electron energies to be employed for positive ion production are in the range of 8 to 12 ev; and for negative ion production, 0.01 to 1.5 ev. Production of positive ions at pressures less than $10^{-4}$ mm is aided by the large cross section of heavy molecules, and is expected to suffice to maintain an arc. In production of negative ions, the electrons must be kept out of the main acceleration region. Analysis indicates that this can be readily accomplished by making use of the great difference in mobility between the electrons and negative molecular ions. Either a magnetron device (Ref. 15 and 16) or a high-frequency alternating electrical field produced between grid wires in the charging region (Ref 17, 18, and 19)can be employed to remove the electrons.

Molecules may also be charged by use of a surface contact ionizer. Since all of the substances under consideration have ionization potentials at least 3 ev greater than cesium, surfaces of higher work function than that of tungsten will have to be employed to produce positive ions. Platinum has a work function of 6.27 ev and could be used as a contact surface only with the compounds of lowest ionization potential. Oxide coated tungsten with a work function of 9.2 ev would give much more complete ionization and is a good operating surface for the comparatively low temperatures, generally less than 600 K, to be employed with the organic compounds. Most of the compounds under consideration, however, are quite reactive and might reduce the oxide surface. Formation of negative ions occurs only on surfaces with work functions less than the electron affinity of the substance. The more active metals, such as barium, are logical choices for the surface, but the reactivity of the propellant material may produce contamination of the surface.

## COLLOIDAL IONS

Many methods have been devised for the production of colloids. Three of these have been selected for detailed evaluation of their applicability in electrical propulsion engines.

The vapor jet rapid condensation process depends on the entropy change resulting from the pressure drop on adiabatic expansion of a vapor to effect sufficient cooling to produce condensation. Analysis reveals the importance of complete and rapid condensation, and indicates that charging agents, such as electrons, mixed with the expanding vapor will aid nucleation and reduce the vapor pressure of the colloidal particles. In this modification of the method, the charging agents can be controlled independently to produce any desired particle size and charge-to-mass ratio, $\alpha$. The choice of

colloid-forming materials depends on the vapor pressure and ease of charging without bond rupture, because fragmentation would produce uncondensable material. Therefore, the most favorable types of propellant materials for colloidal ion formation have been found to be the same as for molecular ion formation, but the operating conditions differ.

Production of charged colloids by electrical atomization depends upon induction of a charge on a liquid and the building up of that charge until the repulsive forces of the charge concentration are sufficient to overcome the cohesive forces of the liquid and, thus, produce a colloidal dispersion. Since the charging and colloid-forming processes are interdependent in this method, adjustment of one affects the other, preventing controlled variation of particle size and $\alpha$. Only positive ions can be produced by this method, and the $\alpha$ values are of the order of $10^{-6}$ electronic charges per amu. Flowrates are $10^{6}$ times smaller than for the vapor jet method (Ref. 20 and 21). The voltage drop and the distance between the source and a ground or negative electrode must be carefully controlled, within limits, as they influence particle size (Ref. 22). This relation would interfere with acceleration of the particles. Because the particles are emitted over a wide angle, up to 180 deg (Ref. 21), focusing of the beam would pose a difficult problem. Furthermore, the conductance and dielectric constant of the liquid must be within certain limits or the material cannot be dispersed by this method (Ref. 22 and 23). A preliminary study has shown electrical atomization as a very simple method of directly producing highly charged colloidal particles, but detailed analysis of the limitations on materials, the inability to control and vary the important parameters of the particles independently, the relation between voltage and particle size, and the problem of focusing the beam argue against use of this method.

Dispersion of powdered solids is another very simple method of producing colloidal particles. Care must be taken to ensure dispersal of the powder as individual particles, possible by the action of electrons in a high-frequency alternating field charging the powder and overcoming the van der Waals forces which hold the particles together.

In both the vapor jet rapid condensation method (since charging can continue by adsorption after condensation) and powder dispersal, some means is required to produce a beam as homogeneous as possible in $\alpha$. This problem has been solved by application of a retarding potential to keep particles in the charging region until their charge-to-mass ratios exceed a given value. This modified source can produce a homogeneous beam of particles traveling in parallel paths and capable of efficient usage of acceleration power. The additional control over $\alpha$ is particularly important because of the impossibility of producing colloid particles of identical charge and mass, like the atomic or molecular ions. A wide distribution of $\alpha$ values would result in inefficient usage of power (Ref. 12).

Some modifications planned for the vapor jet and powder dispersal methods are schematically illustrated in Examples A and C of Fig. 12.

Two methods of charge-to-mass ratio analysis have been adapted for studying the spread of $\alpha$ values of charged colloids, and schematic representations of these modifications are shown in Examples B and D of Fig. 12. The time-of-flight mass spectrograph method of Example D gives the distribution of $\alpha$ values but not the separate charge and mass distributions. This more detailed data can be obtained, as shown in Example B, using a magnetic analyzer to separate the beam according to $\alpha$ values, then employing electron microscope analysis of samples collected for designated $\alpha$ values to give the mass distribution. From the $\alpha$ value and mass distribution data, the charge distribution can be computed. Knowledge of the $\alpha$ mass and charge distributions can serve as a diagnostic guide to aid in elimination of the difficulties in producing a beam of homogeneous $\alpha$.

Figure 12. Charged Aerosol Systems

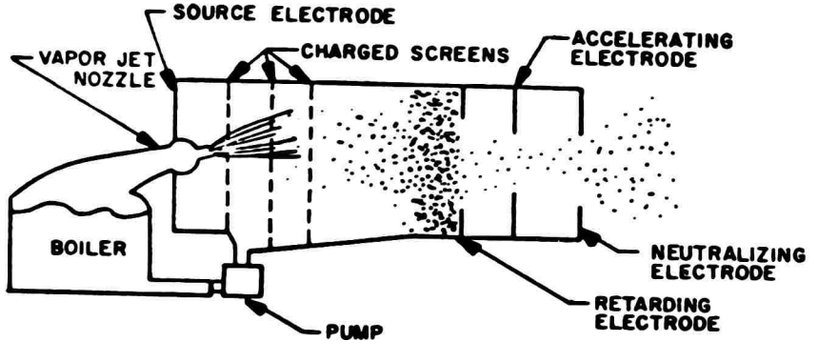


A. PREPARATION: RAPID CONDENSATION OF VAPOR JET
CHARGING: CONTACT OF VAPOR WITH CHARGED SCREENS

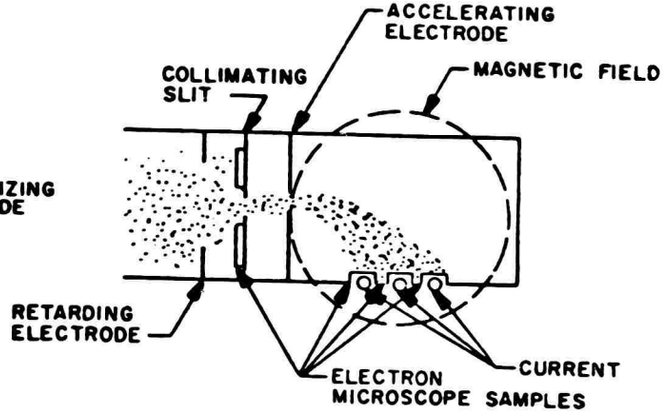


B. MASS SPECTROGRAPHIC DETERMINATION OF $\alpha$ AND COLLECTION OF SAMPLES

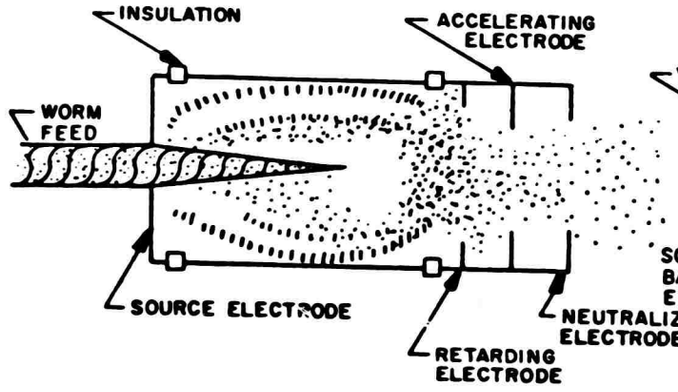


C. PREPARATION: POWDER DISPERSAL
CHARGING: CORONA DISCHARGE

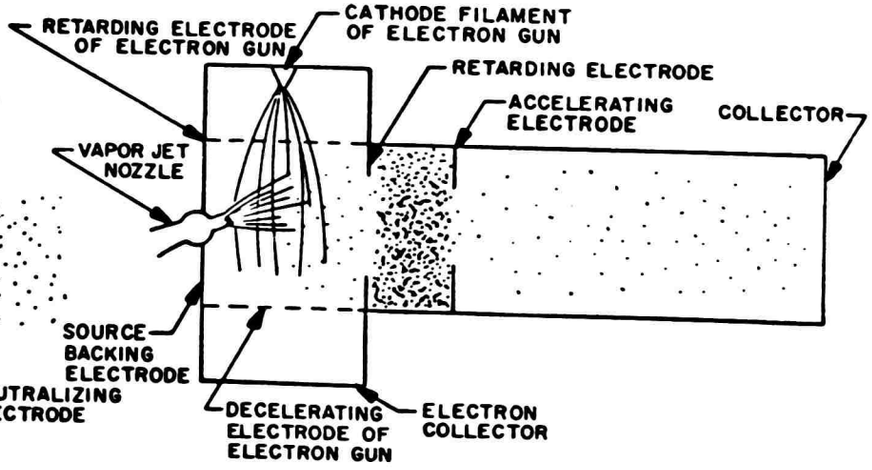


D. PREPARATION: RAPID CONDENSATION OF VAPOR JET
CHARGING: ELECTRON GUN
ACCELERATION: PULSED TIME-OF-FLIGHT MASS SPECTROGRAPH

# MISSION ANALYSIS

## SPIRAL ORBITS

The ion-propelled vehicle is characteristically a low-thrust, low-acceleration system. Because the achievable accelerations are small, compared with the gravitational accelerations existing near planets and the moon, the vehicle's motion is not described by a simple ellipse. If extensive low-thrust maneuvers are to be accomplished, the thrust must be directed nearly perpendicular to the radius vector of the central gravitational force exerted on the vehicle, i.e., circumferential thrust. The trajectory traversed by a vehicle propelled in this fashion is similar to the familiar logarithmic spiral. Depending upon whether the thrust is directed, on the average, with or aginst the vehicle's gross motion, the vehicle will spiral away from or toward the center of gravitation.

The spiral trajectory has been the subject of extensive study at Rocketdyne, and has been discussed in detail in a technical note (Ref. 25). The results have been used to calculate the best set of values for engine parameters for military satellite maneuvers and interplanetary missions. These include orbital transfer, Earth escape, and Earth/Moon transfer. The trajectories have been generated using analytic as well as machine computation techniques. The analyses of other investigators have been surveyed in the literature, and, in some cases, efforts have been directed toward improving them. The machine computations have been developed to include the needs of problems involving three dimensions, all the planets, and a variety of perturbations.

The following discussion covers a portion of the analyses performed on spiral orbits at Rocketdyne. These include the following:

1. Earth escape studies by mathematical analysis
2. Earth escape studies by machine methods
3. Restricted three-body analysis
4. Interplanetary flight studies.

## EARTH ESCAPE STUDIES BY MATHEMATICAL ANALYSIS

A direct application of the information on spiral orbits is the Earth-escape mission. A vehicle may be evaluated for the escape mission by the use of data on payload and flight time versus thrust-to-weight ratio, power, and specific impulse. These data are also applicable, in part, to orbital transfer mission studies, because the first maneuver is to spiral out to the vicinity of the desired orbit.

Analytical solutions to the simple escape spiral from an initial orbit have been derived in the literature by simplification of the differential equations (Ref. 26 and 27). These solutions give a usable estimate of the mass ratio and flight time to escape from an initial circular orbit. Improvements have been made in this method (Ref. 25) during the period covered by this report, so that more information along the trajectory path can be obtained. In particular, data are currently being generated on the propulsion requirements for establishing a circular orbit which is approached from an escape spiral.

## EARTH ESCAPE STUDIES BY MACHINE METHODS

Machine calculations have been developed and utilized for two reasons: (1) to check analytical results, and (2) to find trajectories when many bodies and perturbations are present.

The general problem of motion of a particle under the influence of several gravitational bodies can be approached analytically only in certain very special cases. Therefore, a generalized N-body equation of motion has been prepared to numerically integrate space trajectories with an IBM 709. In this program all pertinent inverse square forces (except the negligible influence of the rocket ship on planetary bodies) are used to calculate the motion of the bodies themselves. This program was used to determine Earth-escape trajectories for several combinations of thrust-to-weight ratio and specific impulse, so that the analytical formulations derived at Rocketdyne and elsewhere could be checked. Some trajectories were run purposely with initial eccentricities. This corresponds to an initial booster error resulting in a noncircular orbit. The data obtained indicate that these eccentricities do not grow larger as the vehicle spirals out. In fact, they tend to decrease, so that injection errors from the boost system will not cause the orbit to behave in an unstable or unmanageable fashion. A sampling of the computer runs is given in Table 2.

The two sources of error in digital calculation are roundoff and truncation errors. The roundoff error is due to the finite number of digits used by the machine, and tends to increase with the number of steps taken in the trajectory. The extended Runga-Kutta predictor-corrector method used by Rocketdyne attempts to reduce the number of steps needed by taking variable steps as large as possible within the accuracy of the machine.

TABLE 2

COMPUTER SPIRAL TRAJECTORY RUNS

| Run | T/W | Initial Orbit Altitude, Miles | Initial Eccentricity | Maximum Calculated Range, Miles |
|---|---|---|---|---|
| 1 | $10^{-3}$ | 300 | 0 | 103,600 |
| 2 | $10^{-4}$ | 300 | 0 | 5,992 |
| 3 | $10^{-3}$ | 500 | 0.0261 | 73,330 |
| 4 | $10^{-3}$ | 300 | 0.0164 | 71.880 |
| 5 | $10^{-3}$ | 1,000 | 0.0966 | 79,770 |
| 6 | $5 \times 10^{-5}$ | 21,000 | 0.0372 | 23,760 |

The truncation error results from taking only a finite number of terms in the infinite series representing the integrated function, and increases with the size of the step. Hence, care must be exercised to minimize the total error.

The computation of trajectories for thrust-to-weight ratios even as low as $10^{-5}$ requires a large number of steps for straightforward integration, so that machine running time becomes prohibitively large. Hence, use of the variations-of-parameters perturbation technique of celestial mechanics is being considered, and a program for the digital computer is being set up. The advantage of this method is that the computation takes large steps in time, reducing machine running time by a factor of 5 to 10, and perhaps reducing roundoff error (Ref. 28). The variations-of-parameters technique is ideal for investigations of cislunar operations. The analytic study of the three-body problem is expected to provide judicious reference orbits for beginning the computation.

On the other hand, variation-of-parameters cannot be as flexible in application to all geometries as straightforward integration of the forces. The present N-body program has been refined and extended in scope to include three dimensions, all solar-system bodies, oblateness of the earth, atmospheric drag, and a routine to provide an estimate of the truncation error.

## VEHICLE ORIENTATION CONTROL

One of the earliest applications of the ion rocket will probably be to control the orientation of Earth satellites and space probes. The need for such control arises as a result of disturbing forces which tend to

cause vehicle rotation or tumbling. Disturbances may be caused by such factors as unbalanced moments produced by rotating powerplant machinery torques resulting from thrust misalignment, or extraneous forces of a nonsymmetrical nature.

To counterbalance the effects of perturbing forces on a satellite or space vehicle so as to maintain a fixed orientation with respect to a particular reference system, it will be necessary to use auxiliary or vernier thrusting devices. Preliminary calculations have shown that the ion rocket is particularly suitable to this usage because of its high efficiency and low propellant consumption, especially for long-lived satellites (such as those intended for observation, navigation or communication) or for Mars-Venus flights. For applications requiring corrective forces of less than about 0.05 lb of thrust, ion motors can be used with electrical energy supplied by low-power generators such as solar voltaic cells, fuel cells or turboelectric systems. For higher thrust level demands, ion motors driven by nuclear turboelectric powerplants will be required.

## PLANAR ORBIT MODIFICATIONS

To ascertain the ability of electrical rockets to perform such missions as satellite rendezvousing and interception, surveillance, and mapping, a comprehensive study was made of thrust requirements and transit times for changing orbital characteristics within the original plane of motion. This investigation basically involves the determination of the effect of a small thrust acting as a perturbation on a satellite orbit, and is detailed in a technical note (Ref. 25). By programed thrusting through various portions of the orbit, the major axis, eccentricity, or perigee angle can be altered. The times required to change these orbit parameters can be estimated from integral approximations about apogee and perigee. Minor orbital

changes can be accomplished rapidly by the use of ion propulsion devices. Major perturbations, however, require the application of thrust for periods of the order of days because of the low thrust-to-weight ratios associated with ion rockets. Thus, large changes limit the ion engine to time-insensitive applications.

## ORBIT INCLINATION

Changing the plane of orbit inclination is of interest for the same reasons as mentioned in the previous paragraph. Since the planar angular rate of change is directly proportional to satellite thrust-to-weight ratio, (Ref. 25), low-thrust ion devices appear to be most useful for maneuvers wherein slow, continuous changes are required. An interesting application in this connection would be satellite probes to continuously monitor environmental conditions such as Van Allen radiation, cosmic rays, and meteorite density. If rapid inclination changes are needed, then higher-thrust rockets such as colloid, arc jet, or chemical rockets will be required.

## PAYLOAD WEIGHT MAXIMIZATION

Limited payload optimization studies for several satellite and space missions have been made during the period covered by this report. For some applications, payload weight is maximized indirectly through the medium of propulsion system weight minimization. Missions of this type usually involve control of a vehicle (or satellite) orientation, or maintenance of a prescribed orbit. Hence, the time of operation (as distinct from the transit time as applied to a maneuver or trip) is the primary independent variable. For example, to maintain a low-altitude orbit constant thrust must be applied over the required lifetime of the satellite to compensate for perturbing forces produced by the oblateness of the earth, the presence of other astronomical bodies such as the moon, and atmospheric drag forces.

Figure 11 shows the competitive operating regimes of several low-thrust systems based on a comparison of propulsion system weight (including propellant) versus required burning time for thrust levels covering the range 0.1 to 5.0 lb. For example, to obtain the minimum powerplant weight for a thrust requirement of 5 lb (corresponding to the atmospheric drag on a 7-ft diameter cylinder in a circular orbit at about 82 mi), an advanced chemical engine ($I_s$ = 330 sec) should be used for maintenance of orbit up to four days, with a plasma jet or colloid rocket for periods up to about three weeks and an ion rocket for times in excess of three weeks. The data from this study contain the latest information on nuclear powerplant weight (including 1000 lb of shielding) as a function of power level, as well as thrust chamber efficiency as a function of specific impulse.

Another mission was analyzed in which a satellite, initially orbiting in a 300-mi orbit, was propelled along a low-thrust spiral to the vicinity of the 24-hr orbit. Data were taken from digital-computer-calculated escape spirals from which it was found that the flight time was inversely proportional to the thrust-to-weight ratio. It was also found that the flight time varied slowly with respect to the specific impulse. Using these data, the vehicle weight was minimized as a function of specific impulse. The optimum specific impulse fell in the operating range of the colloid and plasma engine.

## GENERALIZED MISSION OPTIMIZATION

For many missions of interest, e.g., orbital transfer and interplanetary flight, the multiplicity and complex interdependence of pertinent variables make selection of the optimum operating conditions for payload maximization an exceedingly difficult, if not impossible, condition to satisfy. To simplify calculations, it is often necessary to resort to a reduction in

the number of independent variables by arbitrary assignment of numerical values or particular functional relationships. This computational procedure often yields a limited optimum condition (rather than the best obtainable one) or one which is an unrealizable combination of engine operating parameters.

Serious consideration of possible methods for improving mission optimization techniques has been given. A preliminary study has indicated the potential feasibility of analyzing the complex interdependence of all pertinent variables for particular missions by means of multi-dimensional plots. In this study four assumptions were made:

1. A single, simple, steering program was used, and the engine operated at a constant thrust level
2. The specific powerplant weight was considered to be independent of the power level
3. The vehicle structural weight was taken to be negligible compared with the total vehicle weight
4. The thrust efficiency of the engine was 100 percent.

The result of this analysis is a surface plotted in a three-dimensional coordinate system. This surface is plotted from data obtained through analytic or numerical trajectory studies and the basic low-thrust engine equations. The axes are flight time, specific impulse, and thrust-to-weight ratio. On the surface are inscribed equipayload weight-to-thrust curves. Hence, a point on this surface specifies all of the parameters mentioned above.

From this surface, one may choose an engine operating point for a mission which would be near optimum and yet attainable in practice. Furthermore, the penalty can be deduced for not using the parameters at the optimum

point, and hence, whether it is worth attempting to operate nearer to it. In practice, the use of this technique requires the development of plotting techniques. These might include a three-dimensional model like the P-V-T model for the thermodynamic equation of state, a topographic plot, or triangular plots. It is also desirable to reanalyze the technique taking into account the variable specific weight of the powerplant and the thrust efficiency variations which were eliminated through assumptions 2 and 4.

## ECONOMIC STUDIES

Since the justification for the undertaking of a costly R&D program to produce a new type of rocket engine lies ultimately in the economics of operation, this most important factor is being considered in a preliminary way in current applications programs. If an analytical evaluation indicates that a proposed propulsion system should be capable of delivering payloads on a wide range of missions in acceptable flight times and at costs reasonably below those of available systems, sufficient justification exists for the initiation of a research program to establish technical feasibility. Implicit in this statement, of course, is the assumption that the amortized cost of the R&D program over the expected usage period of the new engine will not radically affect the economics of operation.

It will probably be true that early ventures into space will be undertaken using systems of proven reliability, disregarding the initially greater cost of such systems. However, as the more sophisticated propulsion devices approach the stage of proven reliability, their use will be demanded by economic considerations. For low-thrust electrical propulsion systems, Rocketdyne studies have indicated that two major cost items must be considered: (1) cost to boost the propulsion system plus its payload into Earth orbit, and (2) cost of the electrical propulsion system itself (including propellant). Although first generation ion (and probably plasma

jet) engines should be available within the next three years, systems improved from the standpoint of utility, reliability, and economy will probably not reach operational status before 1965. Therefore, the following discussion of economic considerations is limited to the time period beyond 1965.

Early models of nuclear powerplants for ion rockets are expected to cost between one and ten million dollars each (excluding development cost). This estimate is based on informal discussions between Rocketdyne and Atomics International personnel, as well as a brief survey of the economics of existing reactors. A detailed cost study including such items as reactor type, uranium fuel inventory, fuel element fabrication, coolant inventory and fabrication of other reactor components will be necessary before a reliable cost can be placed on the reactor. Other important cost items of the propulsion system are expected to be the propellant (if cesium is used), thrust chamber (due to the use of refractory and expensive materials), turboelectric components, and radiator. The current price of cesium (propellant) and rubidium (cycle working fluid) is about 500 dollars/lb. This price is expected to drop to between 25 and 100 dollars/lb for ton lot deliveries and ultimately to less than 25 dollars, according to the producers of these metals.

Large chemical boosters, having thrust levels in excess of 1,000,000 lb, should be available in the period beyond 1965. These boosters are expected to be capable of delivering multiton payloads into an earth orbit at costs of 200 to 600 dollars/lb of payload (Ref. 29), depending upon propellants used and the booster payload weight. One analysis (Ref. 30) of the relative payload capabilities of chemical, nuclear, and ion rockets for a Mars mission indicates weights of 4020, 6300, and 8000 lb, respectively, based on initial gross weights of 25,000 lb starting from a 300-mi earth orbit. The booster cost for this accomplishment in each case was

taken to be approximately 40,000,000 dollars. Preliminary cost estimates for this mission are summarized in Table 3. Both the nuclear and ion propulsion systems are assumed to be of an early generation.

Thus, placing these results on an equal basis of cost-per-lb of payload delivered to the Mars orbit, indicates that the ion system is superior because of its greater payload-carrying capability. Since very ambitious missions such as maintenance of satellite orbit or vehicle orientation for extended periods of time, or trips to the more remote planets cannot economically be accomplished by means other than electrical drives, the incentive to develop these systems becomes increasingly attractive.

TABLE 3

PRELIMINARY ECONOMIC COMPARISON OF SYSTEMS FOR A MARS MISSION

| System | Initial Weight in 300-mi Orbit, lb | Mars Payload, lb | Total Vehicle Cost (Includes Booster), $ | Specific Payload Cost, to Mars, $/lb |
|---|---|---|---|---|
| Chemical (2 stages) | 25,000 | 4020 | 10.26 M | 2550 |
| Nuclear | 25,000 | 6300 | 11.55 M | 1830 |
| Ion | 25,000 | 8000 | 13.85 M | 1735 |

## POWER SUPPLY

### ELECTRICAL POWER GENERATORS

A study was made of possible generators to use in a turboelectric conversion system to supply power for the electrical propulsion of rockets. The results of this study are to be published as a technical note (Ref. 30).

Possible propulsion power systems for control and communication at elevated temperatures were explored. The characteristics of known synchronous and asynchronous types of electromagnetic generators were summarized, and some advantages were seen in the Van de Graaf and two - and four-pole electrostatic generators. Semiconductor rectifiers and the use of vacuum tubes were considered in discussion of lightweight transformers and rectifiers to operate at elevated temperatures. It is concluded that from results already obtained in the High-Temperature Electrical System Development program, Contract AF33(600)-35489, operation at 1000 F will be attained, but considering such problems as bearing lubrication, possible radiation damage, radiator size, and turbine blade requirements, new design principles and new materials are needed for operation at higher temperatures.

### CONVERSION OF THERMAL ENERGY TO MECHANICAL ENERGY

A study was undertaken to evaluate various powerplants which could be developed in a three- to five-year period for use as a source of primary power in a 0.1-lb ion engine.

Power conversion equipment to utilize the thermal energy from a SNAP II type nuclear reactor was evaluated for the three systems which seem most promising for early development utilization at the low-temperature

conditions imposed by the reactor of 1300 F maximum coolant temperature. The specification requirements call for a net output of 30 electrical kilowatts for 10,000 v dc and/or 100 v for interplanetary communications. The powerplant is shown in Fig. 13.

Selection of the working fluid for this powerplant is limited to three possibilities because of the near time scale available for complete development and the relatively low reactor coolant temperatures allowable (1300 F). Considered here are sodium-mercury, sodium-helium, and sodium-diphenyl coolant-working fluid systems. The potentially most attractive working fluid, as far as minimum weight is concerned, is rubidium; but because there is little accurate experimental data concerning fluid thermodynamic and physical corrosion properties, an extensive development program is required before this fluid can be considered feasible.

Table 4 is a comparison of the component weights for each system investigated. The direct, reactor-cooled, diphenyl system presents the minimum weight of 1795 lb, including 700 lb of shielding for the nuclear reactor; however, to eliminate the necessity for a new reactor development program for a direct, diphenyl-cooled reactor, the sodium-cooled SNAP type reactor is preferable, with a 90-lb diphenyl boiler weight addition (or 1835 lb). The sodium-helium system weighs 1805 lb, and the sodium-mercury system weighs 1658 lb. The diphenyl working fluid system is considered most feasible if present diphenyl, nuclear, and thermal decomposition data are accurate.

Diphenyl Cycle

The diphenyl system utilizes a Rankine thermodynamic cycle, but because of the shape of the saturation curve on a T-S diagram (Fig 14) the vapor expanding through the turbine becomes superheated. This offers two major

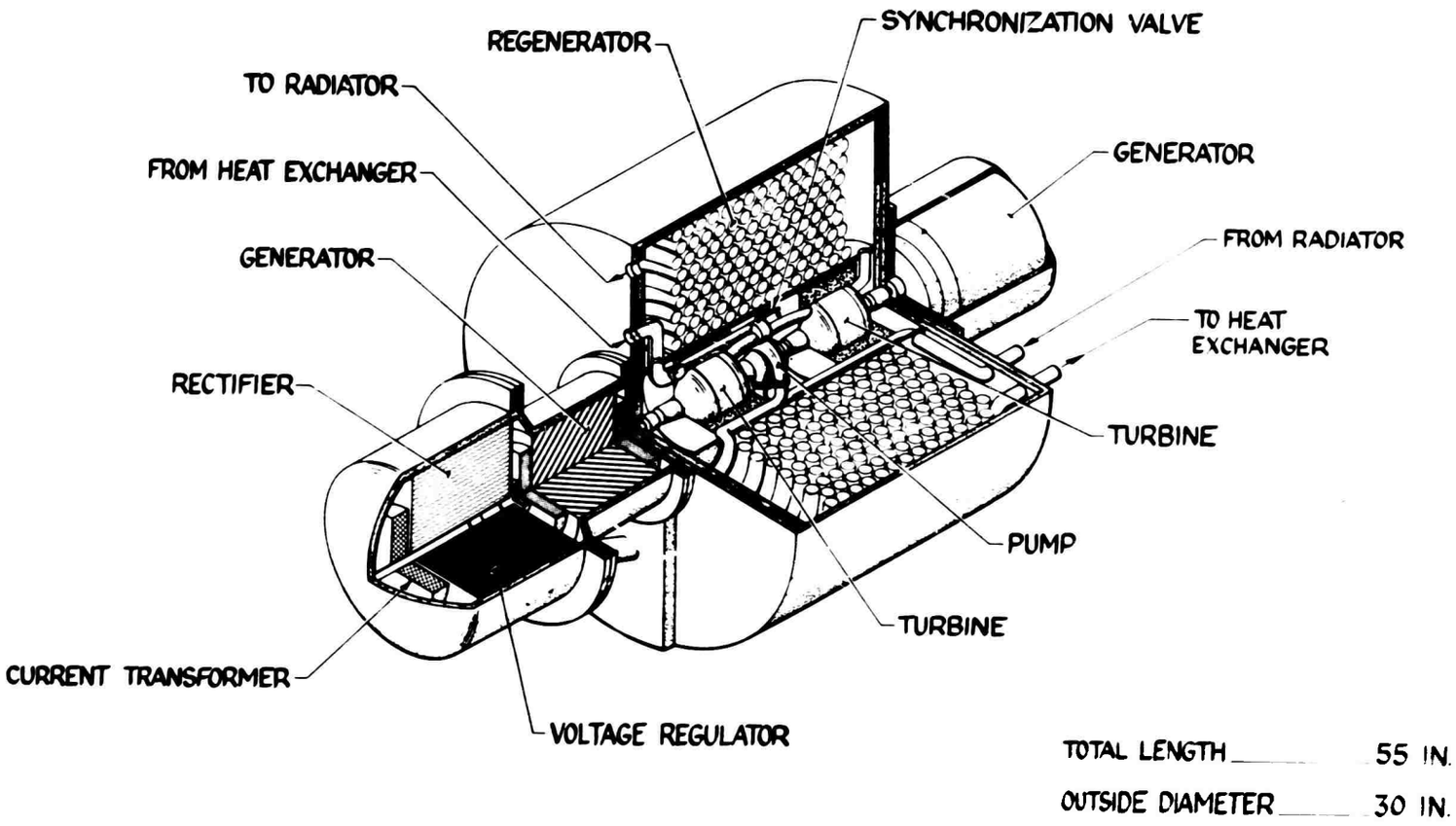


Figure 13. Space Capsule for Powerplant

TABLE 4

WEIGHT COMPARISON FOR SODIUM REACTOR COOLED POWERPLANT SYSTEMS

| Component | Working Fluid, lb | | |
|---|---|---|---|
| | Diphenyl | Mercury | Helium |
| Radiator (dry) | 332 | 278 | 424 |
| Turbine | 83 | 75 | 95 |
| Pump (or compressor) | 10 | 10 | 70 |
| Reactor | 230 | 230 | 330 |
| Heat Exchanger (Na) | 90 | 25 | 56 |
| Regenerator (diphenyl) | 150 | ... | ... |
| Generator | 70 | 70 | 70 |
| Shield | 700 | 700 | 700 |
| Expansion Tank or Sump | 10 | 10 | ... |
| Fluid Inventory | 100 | 200 | Negligible |
| Support Structure, etc. | 60 | 60 | 60 |
| Total Weight, lb | 1835 | 1658 | 1805 |

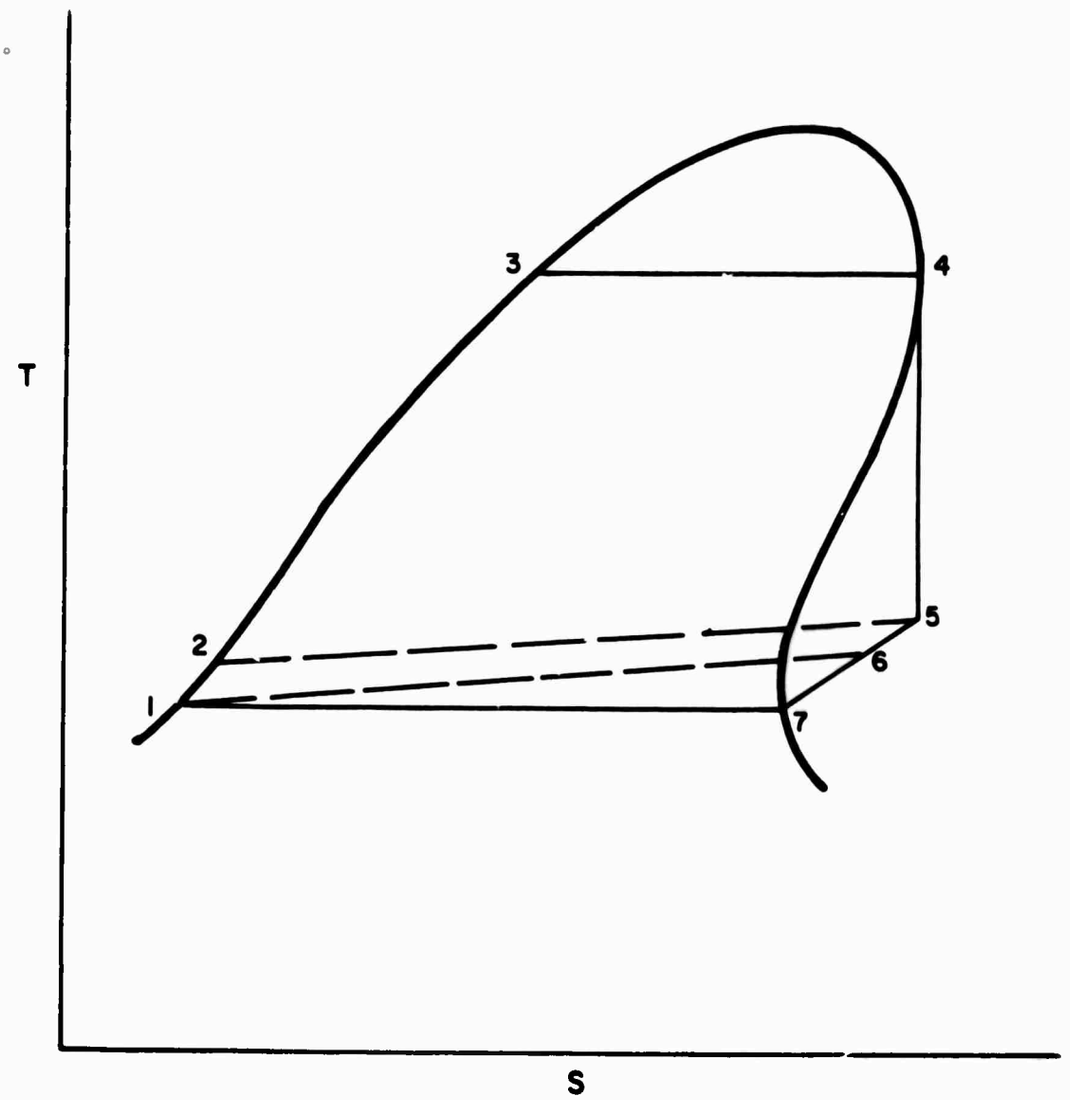


Figure 14. Temperature-Entropy Diagram for Diphenyl

advantages: (1) the turbine always operates with a superheated vapor (see points 3-4 in Fig. 14), and the droplet erosion problem is eliminated, thus adding to long-life reliability, and (2) since the turbine exhaust (point 5) is at a higher temperature than the pump exit temperature (point 1), regeneration of heat is possible from the turbine exhaust gas (points 5-6) to the boiler liquid supply line (point 1-2). The cooled vapor is then condensed in the radiator (points 6-7-1).

Diphenyl is an already proven reactor coolant, although nuclear decomposition rates are appreciable. Because diphenyl is an organic fluid, thermal decomposition is encountered above temperatures of approximately 750 F. These limitations exclude the use of the SNAP II type of reactor for a direct boiling concept, and would, therefore, require a new reactor program for this system, or the utilization of a sodium-diphenyl boiler. The surface area required for the diphenyl condenser-radiator is larger (400 $ft^2$) than that required for the mercury system (143 $ft^2$) since the diphenyl condenser rejects heat at a lower temperature.

The turbine is designed with one to three stages and the physical size is indicated in Fig. 15. In addition, Fig. 16 shows the total weight of the turbine. The efficiency can be maintained at approximately 90 percent in all cases.

Inasmuch as the inlet temperature and the pitch speed remain moderate, the reliability of the turbine stays at a high level. The speed of the turbine is kept at 24,000 rpm.

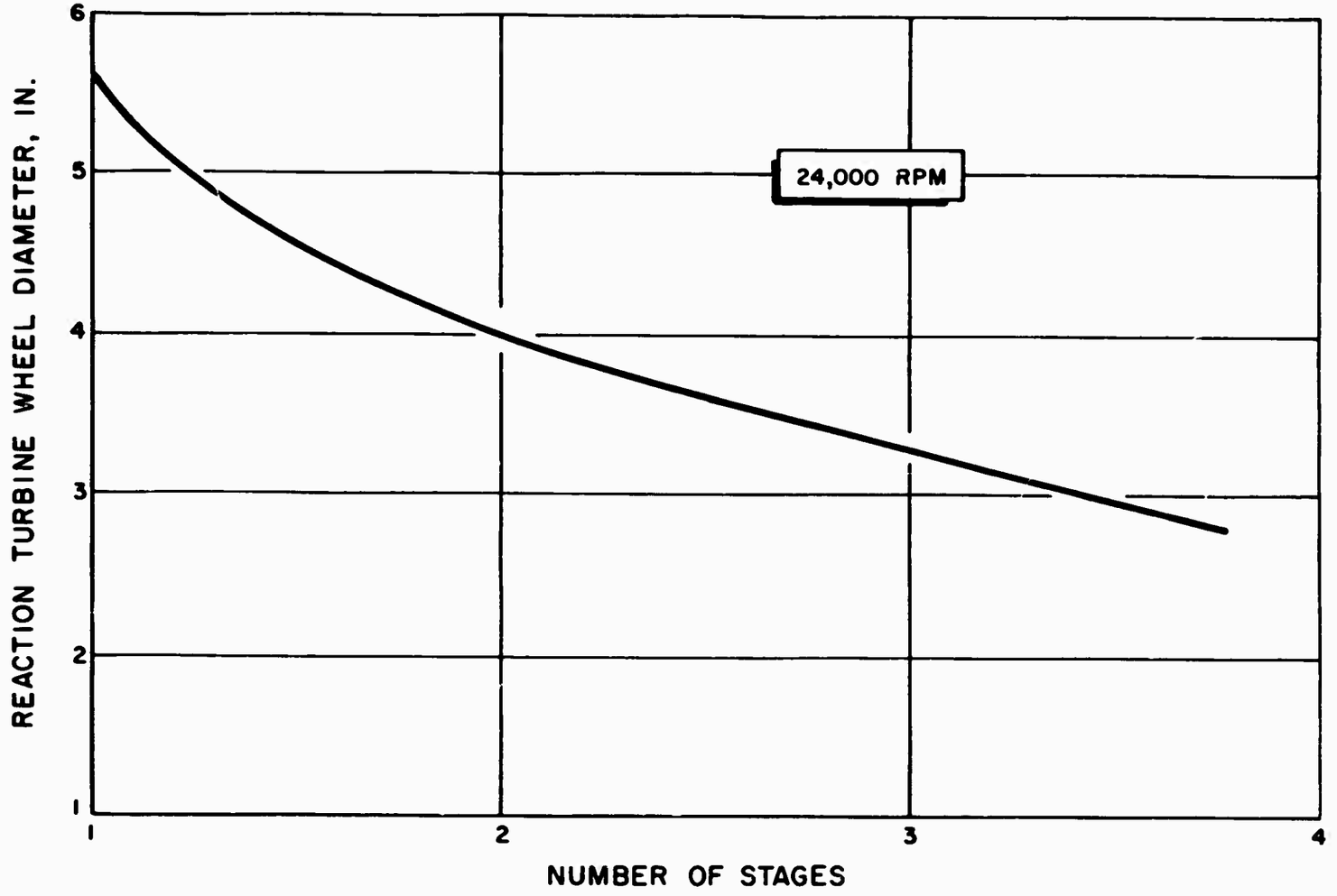


Figure 15. Diphenyl Reaction Turbine Wheel Pitch Diameter

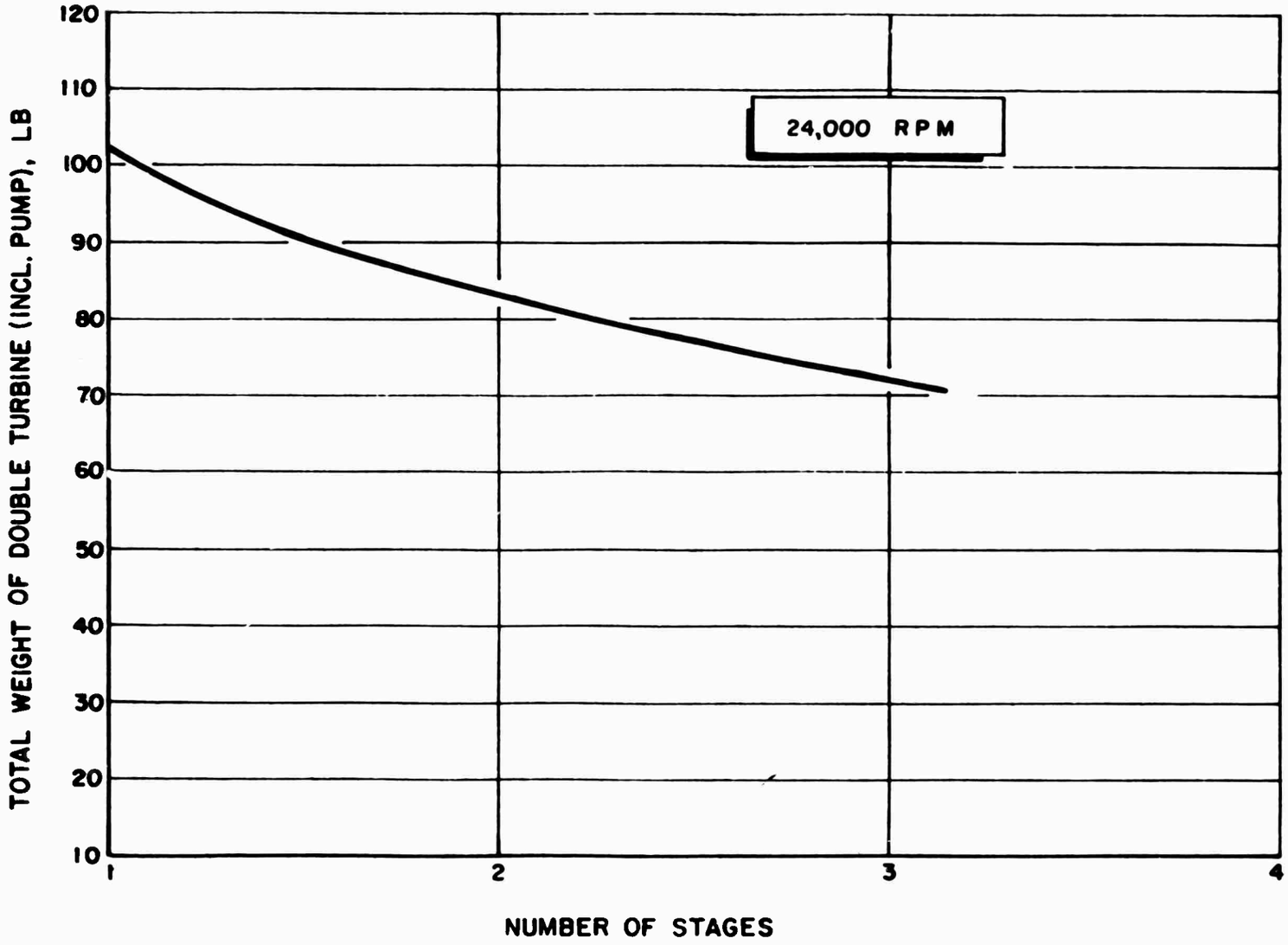


Figure 16. Diphenyl Reaction Turbine Weight

## Mercury Cycle

The sodium-mercury Rankine cycle system was investigated for the conditions described. It is possible to generate either a superheated vapor or a saturated vapor for the turbine within the 1300 F maximum temperature limits imposed. The conditions investigated are given below:

| Turbine Inlet Pressure, psia | Superheat, deg F | Turbine Inlet Temp, deg F |
|---|---|---|
| 200 | 0 | 1017 |
| 200 | 250 | 1267 |
| 400 | 0 | 1148.4 |

Turbine expansion ratios of P1/P2 = 5, 8, 11, and 14 were examined for the conditions mentioned in the table. Fig. 17 indicates the thermal efficiency versus the turbine expansion ratio, which shows little difference in cycle efficiency for the saturated and superheated condition. A higher inlet pressure renders a slightly better efficiency. The efficiency approaches a limiting value shortly beyond an expansion ratio of 14, and is in a range beyond practical use.

Figure 18, shows the moisture content at the turbine discharge, which is significant for long-life applications. Water droplets, for instance, at the nozzle discharge velocity have a great damaging influence upon impact with the turbine buckets. The effect is even more accentuated with mercury droplets of high specific weight. While the maximum moisture content for water is 20 percent, the amount for mercury must be considerably lower. Figure 18 also shows that the moisture content for superheated conditions is considerably lower than for saturated conditions, as would be expected. Superheating the mercury vapor, however, complicates the sodium heat exchanger, and makes it heavier and bulkier, all undesirable features.

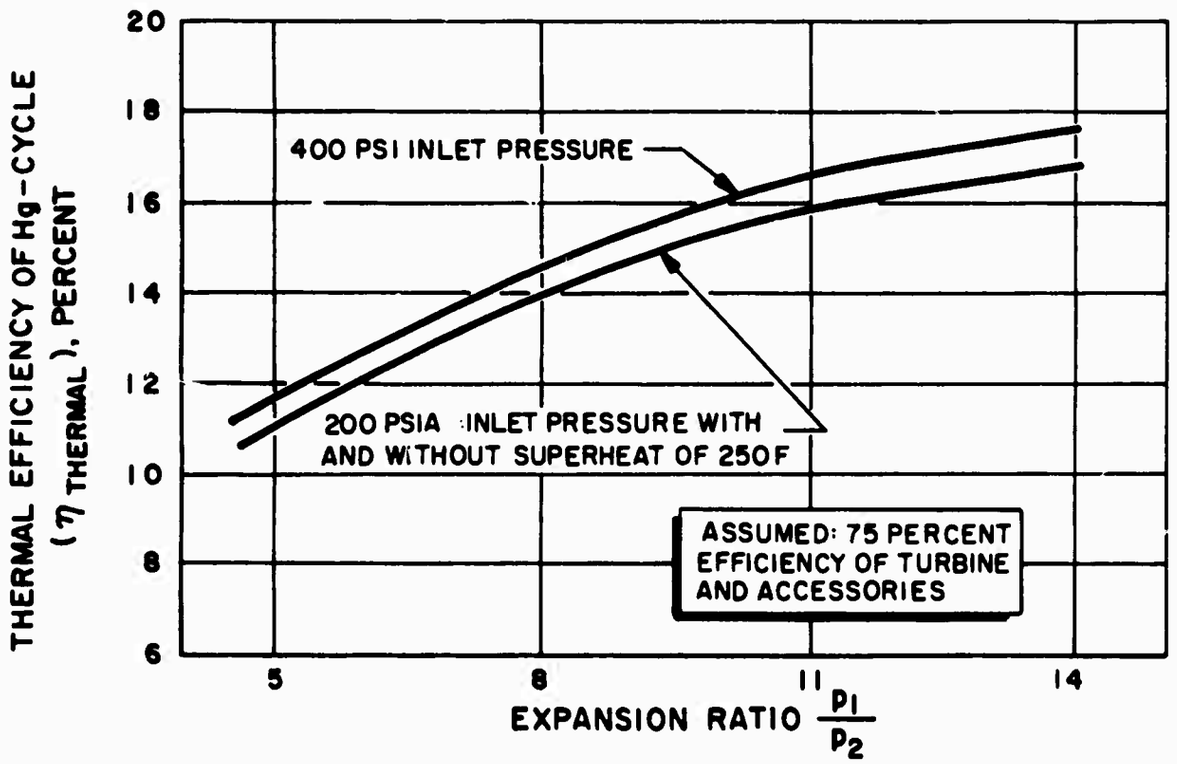


Figure 17. Rankine Cycle of Mercury

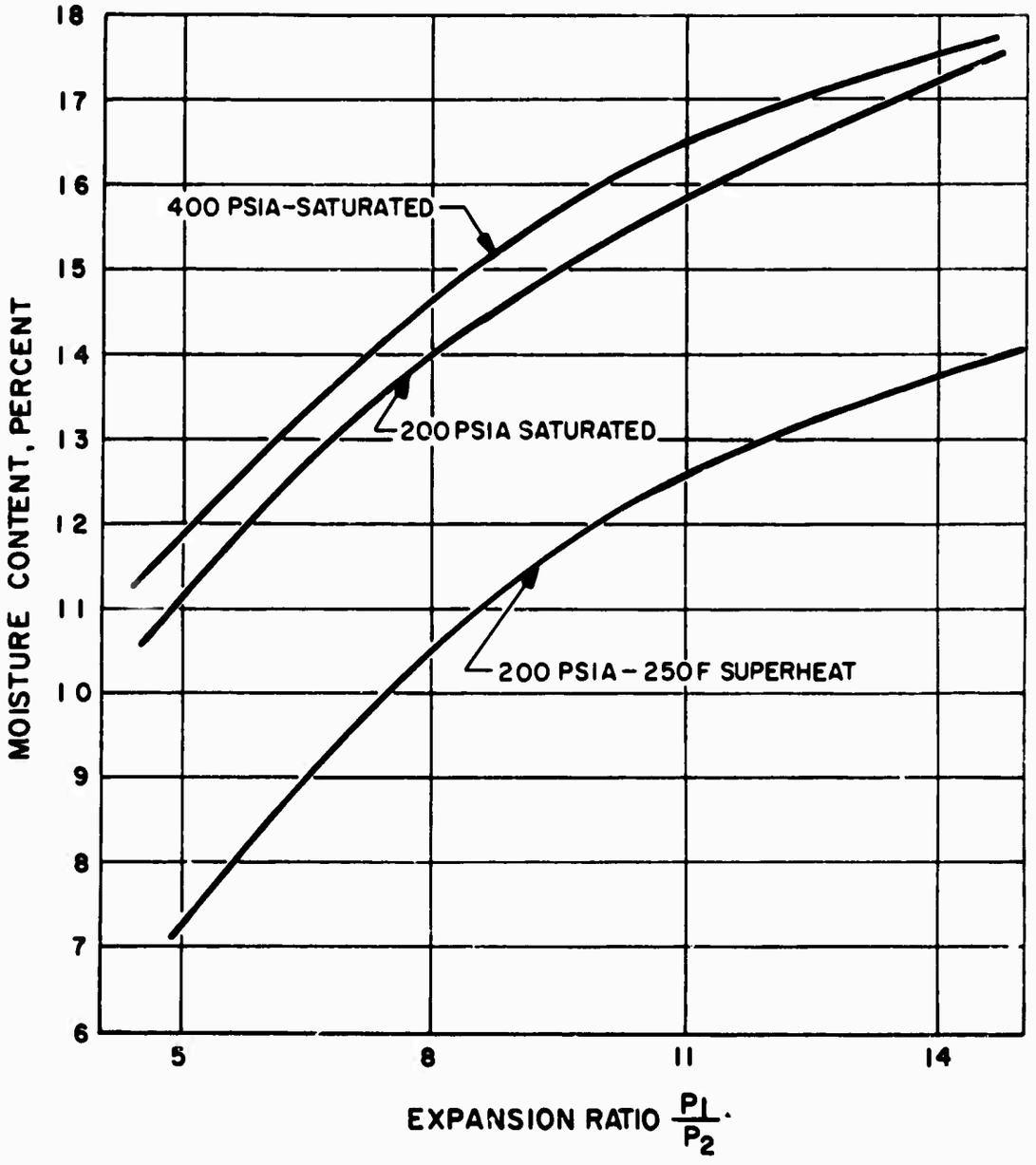


Figure 18. Moisture Content of Mercury Cycle

For a first estimate, all consideration of superheat will be left out. Also, the otherwise suitable radial inflow turbine cannot allow much moisture due to the centrifugal forces on the fluid. It is, therefore, suspected that the droplets of mercury will not leave the turbine, but will collect at the inlet, thereby choking the entrance. This has not been proven, but is highly probable. An axial turbine of conservative design would appear to be the proper solution.

Figure 19, shows the radiator area versus thermal efficiency. It is clearly indicated that the higher the turbine inlet pressure the smaller the radiator area. At the condition selected, the radiator area is 143 $ft^2$, which is small enough that the payload capsule surface area may be utilized for this purpose.

Figures 20 and 21 show the physical size of the turbine in terms of impeller pitch diameter. Figure 20 refers to a single turbine impeller, and 21 to a counterrotating turbine which is to be preferred, inasmuch as it will eliminate most of the rotational inertia. The difference in turbine size is small and can be practically disregarded. The total weight of the turbine is indicated in Fig. 22 and 23. The higher inlet pressure causes a somewhat higher weight, as could be expected, although the difference is not large in relation to the whole system.

The first operating condition ought to be selected on the basis of low moisture content, small radiator area and small turbine size. A good compromise would be to select an inlet pressure of 400 psia, an expansion ratio of 8 or lower, a moisture content of 14.7 percent or lower, and a radiator area of 143 $ft^2$. These conditions are indicated in the diagrams with 0 at the particular design point.

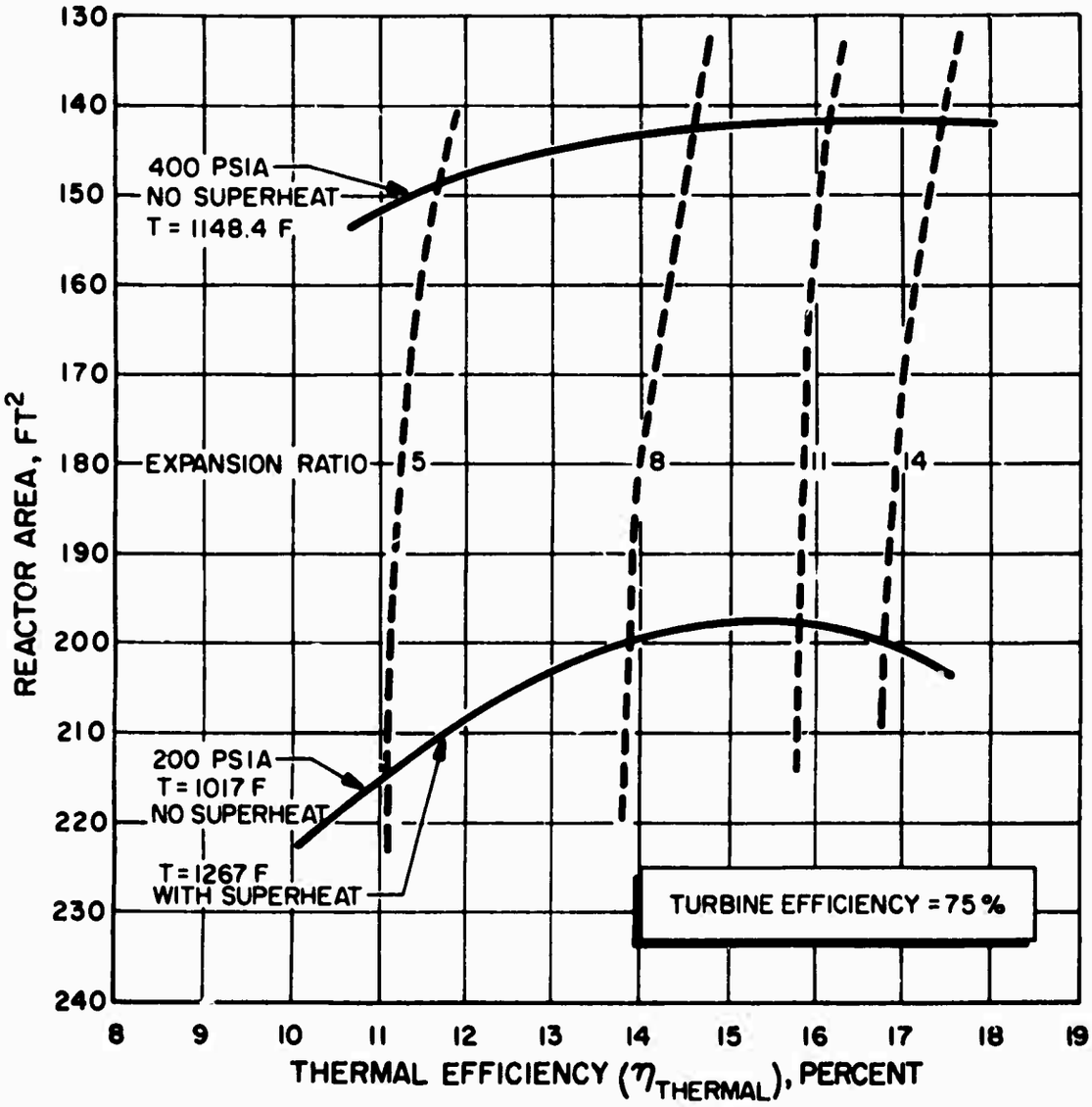


Figure 19. Radiator Size of Mercury Cycle

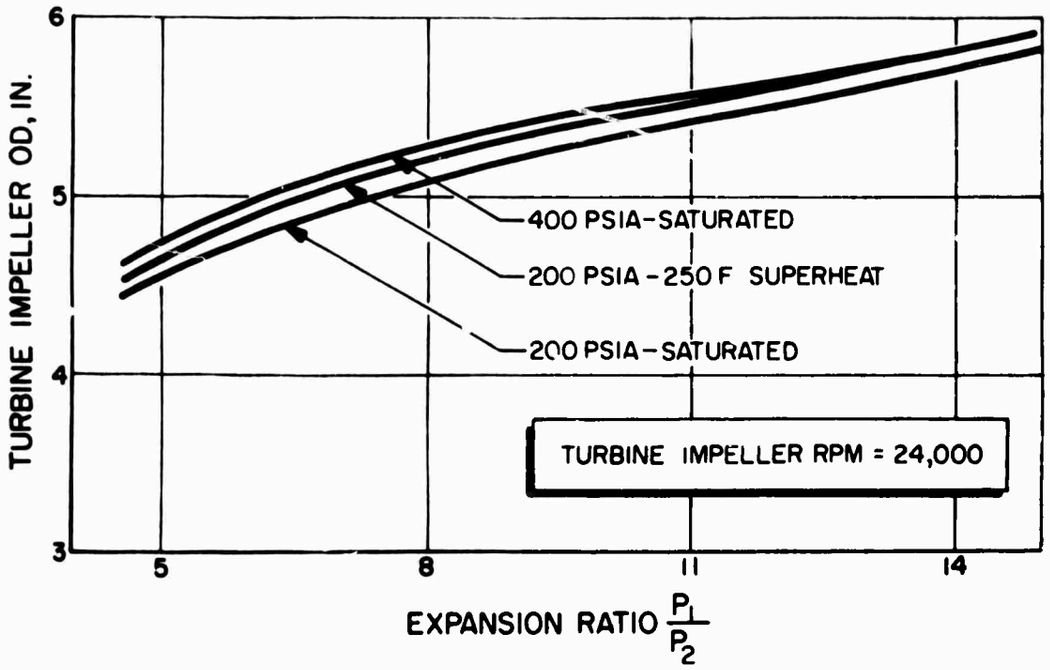


Figure 20. Size of Turbine Impeller of Mercury Cycle

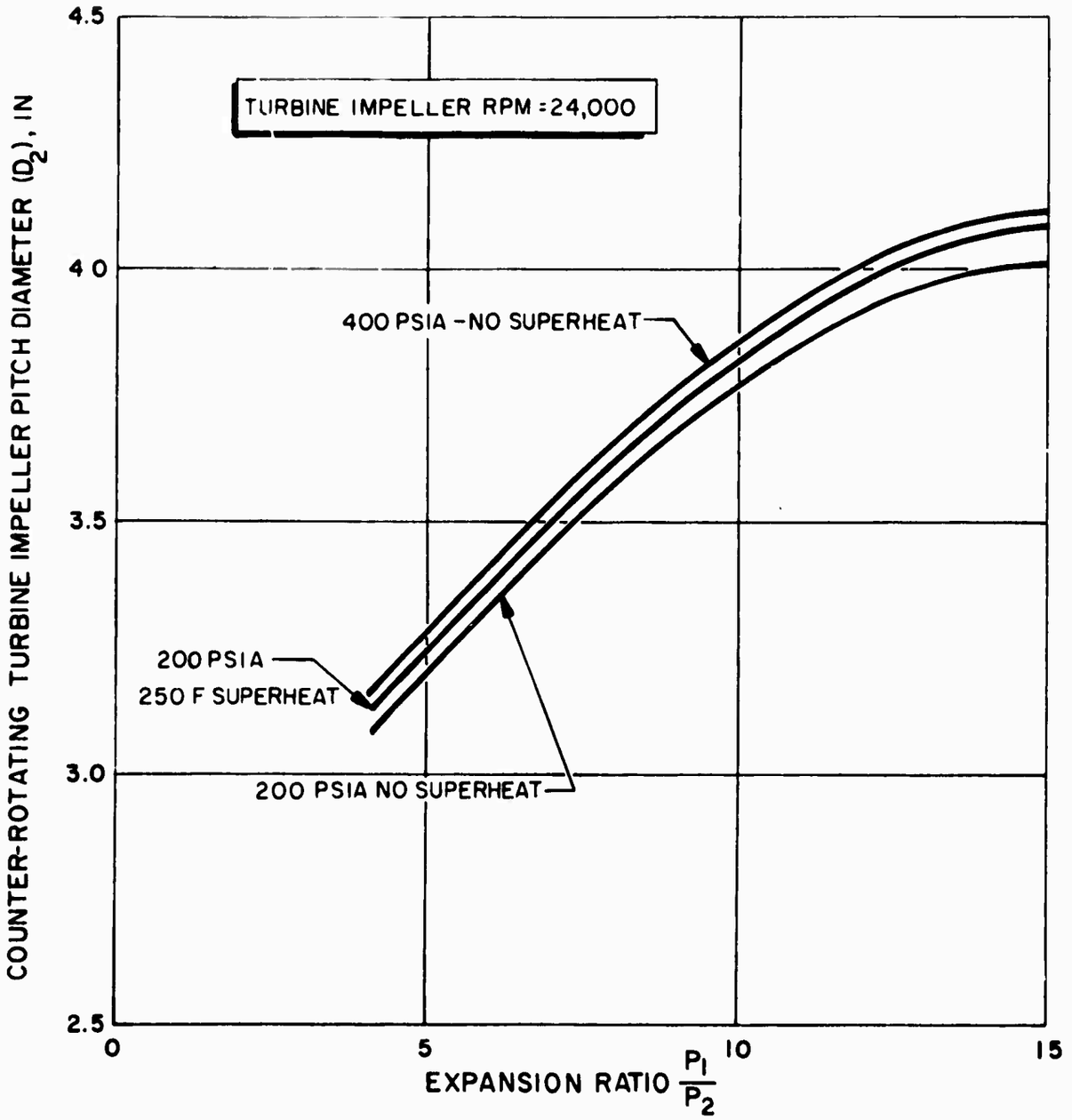


Figure 21. Pitch Diameter of Counterrotating Mercury Turbine.

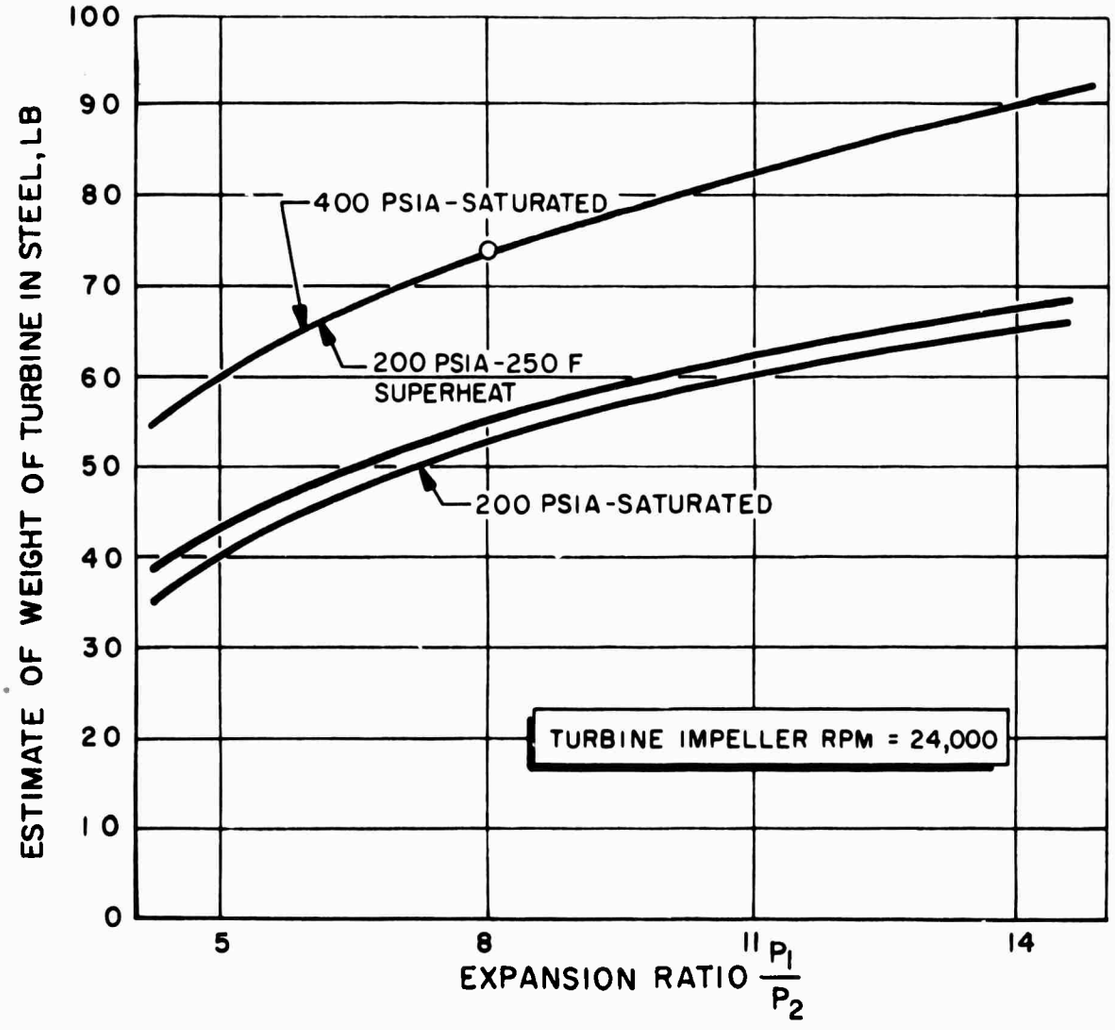


Figure 22. Weight of Turbine of Mercury Cyle

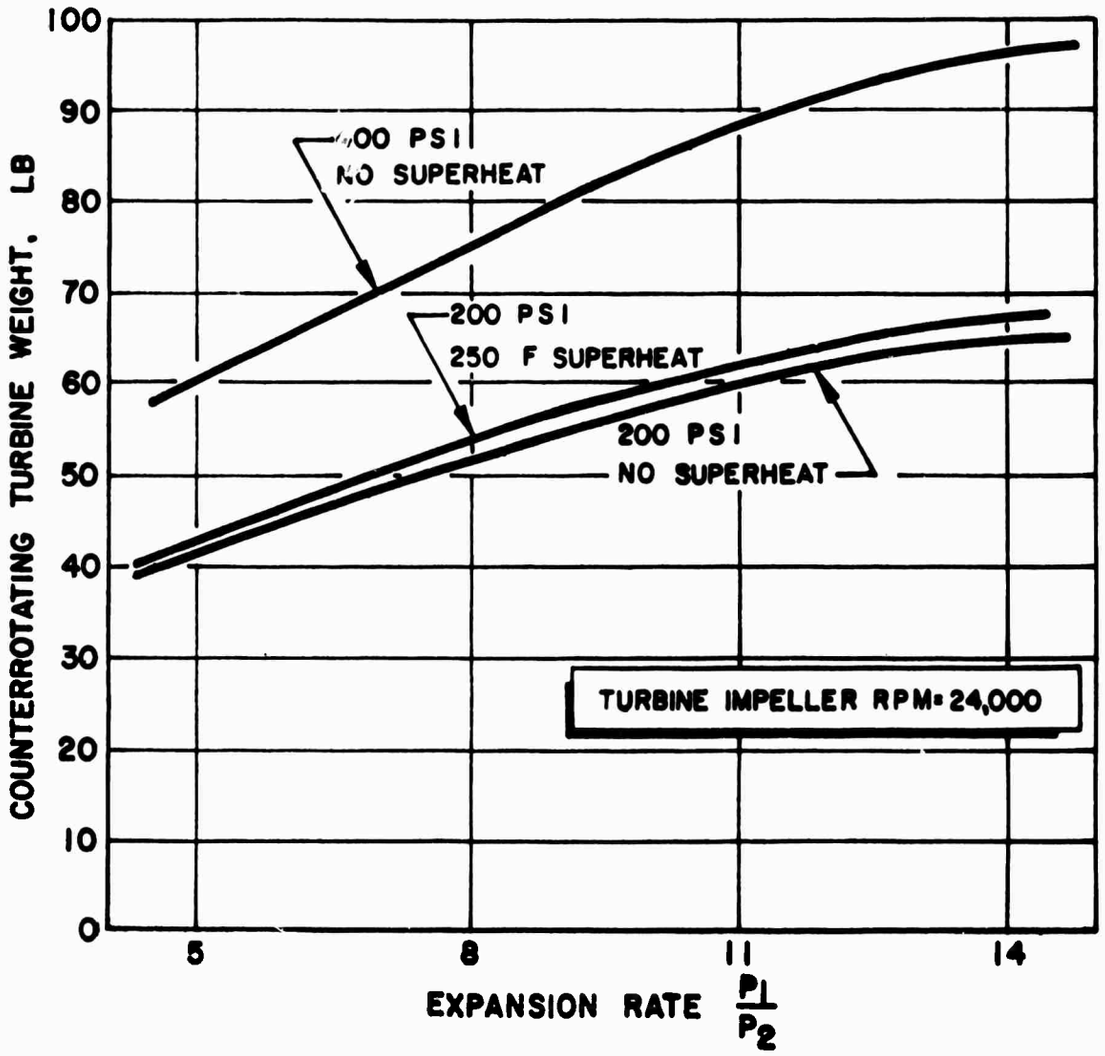


Figure 23. Counterrotating Turbine Weight of Mercury Turbine

The counterflow sodium-mercury boiler was sized for mercury in 1/4-in.-dia tubes and sodium in the shell. The dimensions for a cylindrical form are 9 in. OD and 8 in. long with 256 tubes, resulting in a dry weight of 25 lb for steel construction.

An over-all cycle efficiency of 14.8 percent is obtained with these conditions for an assumed turbine efficiency of 75 percent.

Helium Cycle

The Brayton gas turbine cycle is limited in performance for this application mainly because of the low peak cycle temperature available. Using a sodium-helium heat exchanger, a maximum cycle temperature of 1100 F was assumed. The optimum cycle pressure ratio was found to be 2.0:1, and the minimum radiator area for 30 kw net electrical output is 510 $ft^2$ at a temperature of 140 F. The cycle efficiency for this condition is 11.4 percent.

These results are obtained for the following assumptions:

| | |
|---|---|
| Heat Exchanger temperature | = 200 F |
| Adiabatic Turbine efficiency | = 85 percent |
| Adiabatic Compressor efficiency | = 80 percent |
| Radiator emissivity | = .90 |
| No pressure drops throughout system | |

The physical size of the radiator will constitute a weight disadvantage, and, of course, heavier turbomachinery components.

The helium cycle has been conducted for the purpose of achieving the smallest possible radiator area. This results in a pressure ratio of 2:1 and an inlet temperature of 600 R.

The powerplant was, at first, evaluated for a compressor inlet pressure of 150 psia. This, however, resulted in such a small volume flow that the compressor would have required approximately 300 stages to achieve peak efficiency.

In the next attempt, the volume flow was increased by assuming compressor inlet pressure of 14.7 psia. With this assumption, the compressor required 60 and the turbine 18 stages. The length of the compressor is 60 in., and that of the turbine 27 in. The compressor weight is 70 lb, and the turbine weight is 95 lb, a total of 165 lbs. The speed is kept at 24,000 rpm. The efficiency is 85 percent for the turbine and 80 percent for the compressor.

## RADIATION DAMAGE TO DIPHENYL COOLANT IN A NUCLEAR POWER SUPPLY FOR AN ION ROCKET

The feasibility of using diphenyl coolant as a secondary coolant in a nuclear powerplant depends, among other things, on the extent of decomposition the coolant will incur in the presence of the associated radiation field. A study was made to determine the extent of coolant decomposition, and hence the diphenyl make-up requirement for a particular power conversion system. Since any decision based on a gross underestimate in the damage problem could result in troublesome consequences, it was important to be conservative in this analysis wherever uncertainties were present, while at the same time recognizing that overconservatism might defeat the purpose of this study.

For this analysis, the system was assumed to have the following characteristics:

(a) Reactor power = 500 kw (thermal)

(b) Other reactor characteristics:
   (1) Uranium loading = 12 kg (93 percent $U^{235}$)
   (2) Void fraction = 0.24

(c) Primary coolant: Na or NaK (22 percent Na)

(d) Secondary coolant: diphenyl

(e) G, the quantity of diphenyl decomposition corresponding to a given radiation energy absorption = $0.35 \frac{\text{coolant molecule}}{100 \text{ ev absorbed}}$ = $0.0197 \times 10^{-19}$ lb/Mev = $1.23 \times 10^{-15}$ lb/erg

(f) Weight of Na in heat exchanger = 8.6 lb

(g) Weight of diphenyl in heat exchanger = 10.9 lb

(h) Weight of coolant in radiator = 84 lb

(i) Volume of liquid phase in radiator = volume of vapor phase in radiator

(j) Weight of heat exchanger structure = 90 lb

(k) Configuration as indicated in Fig. 24.

(1) Radiator surface consists of lateral surfaces of Fig. 24

(2) Reactor and heat exchanger locations:

Case I: Reactor at $P_1'$, heat exchanger at $P_1''$, liquid phase of coolant above A - A'

Case II: Reactor at $P_1'$, heat exchanger at $P_1''$, liquid phase of coolant below A - A'

Case III: Reactor at $P_2'$, heat exchanger $P_2''$, liquid phase of coolant below A - A'

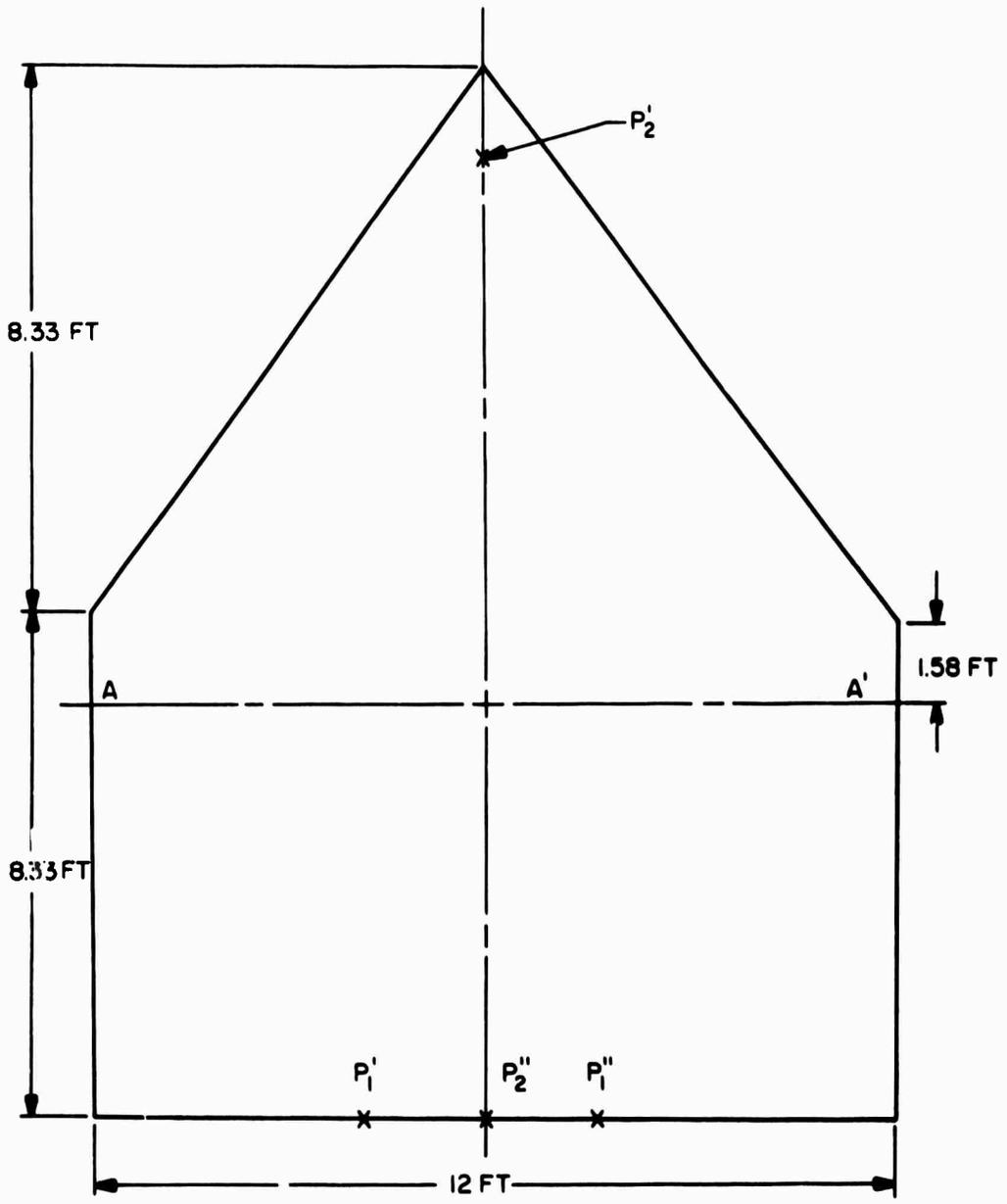


Figure 24. System Configuration

The amount of degradation of the coolant depends, of course, on the locations of the reactor and the radioactive liquid metal coolant. Therefore several reasonable possible locations, as defined above, of these components have been considered. The decomposition of the coolant is due primarily to the following sources:

(a) DHHE (a) — Absorption of the direct beam radiation from the reactor by the diphenyl present in the heat exchanger, with reactor heat exchanger separation equal to a feet.

(b) DBR — Absorption of the direct beam radiation from the reactor by the diphenyl present in the radiator

(c) LMHE — Absorption of the radiation from the radioactive liquid metal by the diphenyl present in the heat exchanger.

The decomposition of diphenyl by the various sources of degradation are listed as follows:

Case I

| | Decomposition Rate (lb/hr) | Overestimate |
|---|---|---|
| DHHE (3 ft) | $9.48 \times 10^{-4}$ | factor of + 5 |
| DBR | $23.1 \times 10^{-4}$ | + 1.5 |
| LMHE | $1.53 \times 10^{-4}$ (Na) | + 2 |
| Total | $35 \times 10^{-4}$ | |

Case II

| | Decomposition Rate (lb/hr) | Estimated Error |
|---|---|---|
| DPHE (3 ft) | $9.48 \times 10^{-4}$ | + 5 |
| DBR | $16.0 \times 10^{-4}$ | + 1.5 |
| LMHE | $1.53 \times 10^{-4}$ (Na) | + 2 |

| Case III | Decomposition Rate (lb/hr) | Estimated Error |
|---|---|---|
| DPHE (14 ft) | $0.58 \times 10^{-4}$ | + 5 |
| DBR | $5.0 \times 10^{-4}$ | 1.5 |
| LMHE | $1.53 \times 10^{-4}$ (Na) | + 2 |
| | $\sim 7 \times 10^{-4}$ | |

If NaK (22 percent Na - 78 percent K) rather than pure Na is used for the primary coolant, the values for LMHE in all cases are reduced to $0.36 \times 10^{-4}$ lb/hr. Furthermore the values for LMHE have been calculated assuming one for the ratio of the time spent by the coolant in the reactor to that spent outside.

It is concluded that the required diphenyl makeup rate for this system is negligible.

## REFERENCES


1. R-847P, Ion Rocket Study Program Final Report, Rocketdyne, a Division of North American Aviation, Inc., Canoga Park, California, 28 February 1958, SECRET.

2. R-1584, AFOSR TR 59-99, Final Report, Ion Rocket Study Program, Rocketdyne, a Division of North American Aviation, Inc., Canoga Park, California, August 1959, SECRET.

3. Langmuir, I and K Blodgett, "Currents Limited by Space Charge Between Coaxial Cylinders," Physical Review 22, 1923, 347-356.

4. Fay, C. E., A. L. Samuel, and W. Shockley, "On the Theory of Space Charge Between Parallel Plane Electrodes," Bell System Technical Journal 17, 1938, 49-79.

5. Langmuir, I., and K. Blodgett, "Currents Limited by Space Charge Between Concentric Spheres," Physical Review 24, 1924, 49-59.

6. R-1763, AFOSR TR-878, Summary of Experimental Ion Rocket Program for the Period 1 May 1958 to 30 April 1959, Rocketdyne, a Division of North American Aviation, Inc., Canoga Park, California.

7. Brewer, G. R., "Formation of High Density Electron Beams," Journal of Applied Physics 28, 1957, 7.

8. Goldman, D. T., and Simon Albert, "Theory of Sputtering by High-Speed Ions," Physical Review 111, 1958, 383-386.

9. Massey and Burhop, Electronic and Ionic Impact Phenomena, Oxford Press 1952, 587-594.

10. R-645P, The Ion Rocket Engine, Rocketdyne, a Division of North American Aviation, Inc., Canoga Park, California, 26 August 1957.

11. Littman, T. M., "Critical Evaluation of the Ion Rocket," Paper presented at Second Symposium on Advanced Propulsion Concepts, AFOSR, Boston, Mass., 7-8 October 1959.

12. WADC TN-59-406, "Ion Propulsion Working Fluid," Rocketdyne, a Division of North American Aviation, Inc., Canoga Park, California, 20 November 1959.

13. Field, F. H., and J. L. Franklin, Electron Impact Phenomena and the Properties of Gaseous Ions, Academic Press, Inc., New York, 1957.

14. Matsen, F. A., "Electron Affinities, Methyl Affinities, and Ionization Energies of Condensed Ring Aromatic Hydrocarbons," Journal of Chemical Physics, 28, 1958 950-953.

15. Sutton and J. E. Mayer, Journal of Chemical Physics, 11, 1943, 56.

16. McCallum, K. J., and J. E. Mayer, Journal of Chemical Physics, 11, 1943, 56.

17. Cravath, A. M., "The Rate of Formation of Negative Ions by Electron Attachment," Physical Review, 33, 1929, 605-613.

18. Bradbury, N. E., "Formation of Negative Ions in Gases by Electron Attachment, Part I. $NH_3$, CO, NO, HCl, and $Cl_2$," Journal of Chemical Physics, 2, 1934, 827-834.

19. Kuffel, E., "Electron Attachment Coefficients in Oxygen, Dry Air, Humid Air, and Water Vapor," Proceedings of the Physical Society, 74, 1959, 297-308.

20. Langmuir, I., O.S.R.D. Report 865, 1942, Office of Technical Services, Washington, D.C.

21. Vonnegut, B., and R. L. Neubauer, "Production of Monodisperse Liquid Particles by Electrical Atomization," Journal of Colloid Science, 7, 1952, 616-622.

22. Drozin, V. G., "The Electrical Dispersion of Liquids as Aerosols," Journal of Colloid Science, 10, 1955, 158-164.

23. Neubauer, R. L., and B. Vonnegut. "Supplement to 'Production of Monodisperse Liquid Particles by Electrical Atomization.'" Letter to the Editor, Journal of Colloid Science, 8. 1953. 551-552.

24. R-1757, AFOSR TN (Number not assigned) "Motion of Low-Thrust Vehicles in a Strong Gravitational Field," Rocketdyne, a Division of North American Aviation, Inc., Canoga Park, California. 1959.

25. Ehricke, K. A., "Comparison of Propulsion Systems; Solar Heating. Arc Thermodynamics, and Arc Magnetohydrodynamics." Advanced Propulsion Systems Symposium. December 1957. 71.

26. Moeckel. W. C. et al. "Satellite and Space Propulsion Systems," NACA Flight Propulsion Convergence, II. 1957. 27.

27. Craig. R. T., et al. "Advanced Space Propulsion Systems," Vol I, Mission Analysis. ER-3622.

28. "Propellant Selection and Design Considerations for Booster Rocket Engine AGC-CR118," Aerojet General Corp., Azusa, California.

29. Kraemer, R. S., and V. R. Larson, "Comparison of Several Propulsion Systems for a Mars Mission," ASME 59-AV-46, March 1959.

30. R-1954. Rotating Power Generation Machinery for Electrical Propulsion, Rocketdyne, a Division of North American Aviation, Inc. Canoga Park, California, 1 February 1960.